To the Graduate Council:

I am submitting herewith a thesis written by Xinan Zhang entitled "Characterizing Strength and Fracture of Wood Micropillars Under Uniaxial Compression." I have examined the final electronic copy of this thesis for form and content and recommend that it be accepted in partial fulfillment of the requirements for the degree of Master of Science, with a major in Forestry.

Siqun Wang
Major Professor

We have read this thesis and
recommended its acceptance:

Timothy M. Young

Qiuhong Zhao

Acceptance for the Council:

Carolyn R. Hodges
Vice Provost and
Dean of Graduate Studies

(Original signatures are on file with official student records)

Characterizing Strength and Fracture of Wood Micropillars Under Uniaxial Compression

A Thesis
Presented for the
Master of Science Degree
The University of Tennessee, Knoxville

Xinan Zhang
August 2008

ACKNOWLEDGEMENTS

I give thanks to my major professor, Associate Professor Siqun Wang, for ideas, inspiration, guidance, support, encouragement, and patience throughout this thesis work. I am also grateful to Dr. Tim Young and Dr. Qiuhong Zhao for being my committee members.

I appreciate the opportunity to conduct a part of my project in Oak Ridge National Laboratory (ORNL) through the HTML User Program Project #2006-054 approved by Dr. Edgar Lara-Curzio. I am appreciative of the financial support provided by the USDA McIntire-Stennis Cooperative Forestry Program, the USDA Wood Utilization Research Grant and UT Department of Forestry, Wildlife and Fisheries.

I thank Dr. Xing Cheng for his help with the initial sample preparation process of microtoming. I would also like to thank Dorothy Coffey at ORNL for her assistance with FIB milling. I also give thanks to Dr. John Dunlap at UT for training me on proper use of the SEM. I am also grateful for the help from Dr. Edgar Lara-Curzio, Rosa Trejo and Laura Riester during the micro-compression testing and nanoindentation.

Finally, I would like to thank my family for the support and encouragement they have given me throughout my college career. I greatly appreciate the love and support of my wife Ping Chen. I am looking forward to the start of our new careers together.

ABSTRACT

The structure of the actual wood cell wall is very complex and it consists of several layers. Some research has been done to measure the mechanical properties of wood cell wall. For example, the hardness and modulus of wood cell wall was estimated using a nanoindentation test. But the mechanical contribution of wood cell wall is not fully understood and documented in the literature. Understanding the micro mechanical properties of the wood cell wall are paramount because of the potential for applications in cellulose nano-composites research and development.

The focus of this research was to investigate the essential of the strength and fracture of wood cell walls by uniaxial micro-compression test. Keranji and loblolly pine were chosen to perform the micro-compression tests. After initial sample preparation by microtoming, a novel method for sample preparation was adopted. The cylindrical shaped micro pillars were milled using a Focused Ion Beam (FIB) while each pillar was milled in a single wood cell wall. The beam voltage of this FIB system was 30 KV. After measuring the dimension of the micropillar through analyzing the SEM images by ImageJ software, the uniaxial compression test on the micro pillar was conducted using a Nano II Indenter system with a 10 micrometers diameter flat tip. The loading rate of 20 nm/s was used to obtain the load-displacement curves. As a result, the yield stress of keranji cell wall was 136.5 MPa and the compression strength was 160 MPa. The yield stress of loblolly pine cell wall was 111.3 MPa and the compression strength was 125

MPa. The fracture behavior of wood micropillar confirmed that wood cell wall also is a brittle type of material.

KEY WORDS: wood, cell wall, loblolly pine, keranji, focused ion beam (FIB), scanning electron microscopy (SEM), micropillar, uniaxial micro-compression test, fracture behavior.

TABLE OF CONTENTS

LIST OF TABLES

LIST OF FIGURES

CHAPTER 1 INTRODUCTION

1.1. Background

As one of the most important and people's favorite raw material in the world, wood has been used in wide varity of applications such as construction, decoration, furniture making and paper manufacturing for a long time. The physical and mechanical properties of commercial grade timbers have well been studied and documented.

It is well known that wood is nonhomogeneous in the macro, micro and nano scales (Stokke and Groom 2006). The wood cell wall is a complex composite consisting of cellulose, hemicellulose and lignin. The wood cell wall can be divided into the primary cell wall layer and the secondary cell wall layer. The three different layers comprising the secondary cell wall are S_1, S_2 and S_3 (Figure 1-1). One of the differences among these layers is the Micro Fibril Angle (MFA). This angle is approximately 50 º to 70º for S_1, 10 º to 30º for S_2 and 60 º to 90º for,S_3.

Wood plastic composite is a good example of the utilization of the cell wall component. So the mechanical properties of the wood cell wall are important and further research is warranted as related to cellulose nano-composites. currently, knowledge of the properties of the wood cell wall is incomplete, the mechanical contribution of wood cell wall is still not fully understood (Keckes et al. 2003) .

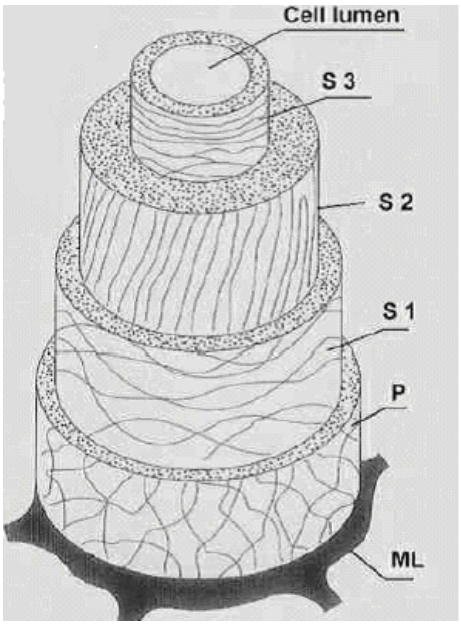

Figure 1-1. Schematic model of the cell wall layers

Some researches have been done as related to the nanoindentation test. The stiffness and hardness of wood cell wall could be measured through this technique. However there are still some limitations to this test. The accuracy of this nanoindentation test data is skeptical. First, as it is well known, the formula used in the Oliver and Pharr method (Oliver and Pharr 1992) to calculate the stiffness and hardness from nanoindentation test is focused on homogeneous materials. For wood material, because the MFA in the wood cell wall is different, the wood cell wall is actually the anisotropic and heterogeneous material. Second, the Poisson's ratio in the formula was chosen for timber. Whether the Poisson's ratio of the timber is the same as the one of wood cell wall is unclear. So it is important to find new way to investigate other properties of the wood cell wall such as compression strength and yield stress which can help us understand it better.

1.2. Objectives

This research investigated the properties of the wood cell walls such as yield stress, compression strength, and fracture behavior through uniaxial micropillar compression test.

The main goals of the project were to:

1. Introduce a novel method for wood cell wall sample preparation, which is to mill a micropillar in a single cell wall by Focused Ion Beam (FIB).
2. Perform uniaxial micro compression test on the pillars.
3. Investigate the fracture behavior of micropillar.
4. Measure the yield stress and compression strength through micropillars compression test.
5. Compare the engineering modulus from micro-compression test and the modulus from nanoindentation test.

1.3. Rational and significance

This thesis introduced a useful method for wood cell wall specimen preparation. The sample was prepared by microtoming and then was milled using the FIB system. The cylindrical shaped micro-pillars were fabricated from these methods. Using the uniaxial

compression test, the yield stress and compression strength of the wood micropillars were measured. The fracture behavior of the wood micropillar was further investigated from SEM imaging.

These properties of wood cell wall are investigated for first time in this thesis. No previous research in this area has not been found. The reasonable force to compress the wood cell wall will be helpful to understand how much load should be used to break wood in cell wall level. In addition, computer simulation of wood structure is a popular research to predict the properties of timber, but the essential properties of wood cell wall should be discovered first because this is the foundation. Understanding and quantifying these wood cell wall properties will be important when the wood cell wall is used as a component of wood based composites in nano- or micro- scale applications. This thesis will advance the research of the properties of wood cell wall.

CHAPTER 2 LITERATURE REVIEW

2.1. Introduction

A wide range of reference was reviewed to find a novel way to discover the strength and fracture of wood cell wall. First, the important mechanical properties of timber which focused on the traditional compression strength were reviewed. Second, a review of the nano- and micro- properties of the wood cell wall, most of which using the nanoindentation test was introduced. This review of the literature suggested that essential properties of the wood cell remain undiscovered. Third, the FIB system and its comprehensive applications as related to wood material was reviewed. Finally, the micro-pillar compression test as related to the metal based materials compression properties was reviewed.

2.2. Important mechanical properties of wood

Mechanical properties are usually the most characteristics of wood products to be used in structural applications (Bowyer et al. 2003). Various mechanical properties of timber are measured using a variety of tests. Modulus of elasticity (MOE), modulus of rupture (MOR) and shear strength are obtained using a bending test. Tensile strength parallel to grain can be estimated by a tensile test whereas compression strength (parallel to grain or perpendicular to grain) can be measured by a compression test.

Much research has been conducted on the wood bending test. Yoshihara and Tsunematsu (2007) examined the bending and shear properties of compressed wood Sitka

spruce. Korkut and Guller (2008) determined physical and mechanical properties of European Hophornbeam wood. Gomez and Svecova (2008) tested full-scale Douglas-fir in three-point bending test after strengthening with GFRP sheets, the beams failed at horizontal shear force within the range of 150-266 kN by debonding of shear reinforcement. Seeling (1998) performed bending test on Hickory (Carya ovata K. Koch) which grew in Germany. Bending strength and stiffness showed that Hickory delivers wood with an enormous strength potential in Germany under optimal growing conditions.

Shupe et al. (2007) tested MOE and MOR of Chinese tallow tree through a bending test, it was found that Chinese tallow tree has sufficient bending strength for low to medium structural uses. Cockrell and Knudson (1973) found that compression wood of the giant sequoia had higher values than normal wood (NW) in crushing strength and ultimate stress in tension parallel to grain, in toughness, in MOR, and in work to maximum load and total work in static bending. Yoshihara and Kubojima (1998) examined the applicability of Timoshenko's theory and proposed an empirical equation to derive the shear modulus property by a static bending test.

Macro-scale compression test is a traditional way to measure mechanical properties of wood materials. Wood is a true composite material with orthotropic and anisotropic properties. The compressive strength parallel to grain is much higher than the one perpendicular to grain. Eberhardt (2007) studied compression test on southern yellow pine and found that the compression strength is greatest in the longitudinal direction.

Most compression tests are performed parallel to grain. Yoshihara and Yamamoto (2004) did compression test on Buna to determine the compressive properties in the grain direction. Boey et al. (1985) found that the compressive strength of Kapur was improved by imputing polymeric monomers into the wood cellular structure. The United States federal highway administration performed full-scale tests on dry southern yellow pine timbers in compression parallel to the grain, finding that the default strength of clear wood at 12 percent moisture content is 52.7 MPa.

Lourenco et al. (2007) evaluated the compressive properties of chestnut under compression perpendicular to grain. The samples included both new (never been used structurally) and old (obtained from structural elements belonging to ancient buildings) chestnut. They found that the load history and time do not change the mechanical and physical properties of chestnut. However the orientation of the loading direction with respect to the annual growth rings must be taken into account.

Hoffmeyer et al. (1989) introduced a model which links the mechano-sorptive behavior of wood subjected to high compression stresses parallel to grain to the formation of slip planes in the cell wall. Hong and Barrett (2006) did compression test on Douglas-Fir and developed a three-dimensional wood-related material model which showed good capability of three-dimensional finite element analysis of wood behavior.

Kucera and Bariska (1982) studied the failure forms in spruce and aspen wood samples caused by axial ultimate compression stress. The failure morphology of the

individual cells of the xylem may be explained to some extent by their geometry. The anatomical features of the wood species were the most influential factor for fracture morphology (Bariska and Kucera 1985).

Shipsha and Berglund (2007) found that in the transverse compression test, the measured displacement and strain fields in the radial–tangential (r–t) plane of a wood board containing the pith region are strongly non-homogeneous. Hwang et al. (2001) investigated the relationships between the compression strain and fracture, and increases in ambient temperature of the wood surface. They found that, in the longitudinal compression test, the location of the surface temperature rose closely corresponding with the site of fracture of the specimen. While in the test of lateral compression, the temperature rise on the surface of the wood specimen was not significant within the proportional limit but increased significantly with increasing compression strain above the proportional limit.

Gong et al. (2004) investigated the compressive properties of wood-cement particle composites and found that it has the capability to absorb energy. The phenomenon that the mechanical properties were not isotropic indicates directional dependencies due to the orientation of the wood particles caused by pressing during the manufacturing process. The larger strain at peak load showed that the wood-cement particle composites can be used for applications where energy dissipation is highly required.

2.3. Nano and micro mechanical properties of the wood cell wall

Recently, some research has investigated the mechanical properties of the wood cell wall at the micro- and nano- scale. Orso et al. (2006) conducted beam bending experiments on cantilevers which were cut with the FIB from spruce wood cells. The cantilever was tested by applying a known force with a piezoresistive tip that was mounted on a micromanipulator. According to this method, the elastic modulus of spruce wood cell wall is about 28 GPa. Cheng (2007) performed a nano-scale three-point bending test on the individual fibrils by Atomic Force Microscope (AFM), these fibrils were generated from cellulose by high intensity ultrasonic treatment. The elastic modulus of fibrils with diameter from 150 nm to 180 nm was approximately 98 GPa. Navaranjan et al. (2008) performed bending tests on single wood pulp fibers by a new method based on AFM using a modified cantilever probe. Results indicated that earlywood fibers have a greater range of flexibility values than latewood fibers.

Relative to the reference cited previously, more research has focused on the nanoindentation test. Wimmer (1997) was the first to prove the capability of nanoindentation to determine the mechanical properties of cell walls in wood. This was a novel technique where an indenter penetrated the sample of a material. The penetration depth and load can be recorded during this indentation. This resulted in an estimate of the stiffness and hardness at the indented location.

It was found that there is no significant difference between modulus values inferred from nanoindentation and those obtained from single fiber tensile testing (Lee et al. 2007a). Hardness and elastic modulus values were higher in the longitudinal direction than those in the transverse direction. Increasing the holding time led to an increase in indentation displacement and a decrease in hardness.

Normally the specimen for the nanoindentation test should be embedded in epoxy resin and smoothed by microtoming to get a flat surface. Jakes et al. (2007) developed a method to prepare surfaces suitable for nanoindentation on the transverse plane of wood cell walls without embedment, grinding or polishing. This method also minimizes alterations of cell wall properties. When the data was analyzed, the indentation areas were determined using both the Oliver-Pharr method (Oliver and Pharr 1992) and a calibrated AFM. Through this experiment, they found no strong evidence that an indentation size effect was present in either H or E_r.

The difference of MFA may result in different mechanical properties. Gindl et al. (2004) did nanoindentation on Norway spruce cell walls with highly variable cellulose MFA and lignin content. They found that the elastic modulus of the secondary cell wall decreased significantly with increasing MFA. Tze et al. (2007) reported the continuous nanoindentation measurement of longitudinal stiffness and hardness of wood cell walls as the indentation progresses. They did the nanoindentation on 10 different annual rings with the MFA between 14° and 36°. The mechanical values were found as a function of MFA, which implies that both the longitudinal modulus and hardness decreased while the

MFA increased. As a result, they advised for future research that samples be taken from the same growth ring to minimize any unintended variations, therefore, any treatment-induced changes in the cell wall can be identified.

The interface properties of wood based composites are another popular area. Konnerth and Gindl (2006) prepared spruce wood with four different adhesive bonds for nanoindentation testing. Both hardness and elastic modulus of interphase cell walls from melamine-urea-formaldehyde (MUF) adhesive bonds increased. Hardness of interphase cell walls from phenol-resorcinol-formaldehyde (PRF) adhesive bonds improved as well. But hardness and elastic modulus of cell walls from the interphase region in polyvinylacetate (PVAc) and one-component polyurethane (PUR) bonds showed lower elastic modulus and hardness. In another project, a grid nanoindentation mapping experiment of a wood phenol–resorcinol–formaldehyde adhesive bond was done (Konnerth et al. 2007). The modulus of elasticity of the adhesive was clearly lower than the modulus of wood cell walls, whereas the hardness of the adhesive was slightly higher compared to cell walls. They thought the unexpectedly high variation of the modulus between 12 and 24 GPa may be explained by the interaction between the helical orientation of the cellulose microfibrils in the S2 layer of the wood cell wall and the geometry of the three-sided Berkovich type indenter pyramid used. Both trends of changing mechanical properties of wood cell walls with varying distance from the bond line are attributed to effects of adhesive penetration into the wood cell wall.

Using nanoindentation tests on spruce wood samples which were infiltrated with a melamine–formaldehyde resin, Gindl and Gupta (2002) found that melamine treatment of wood improves mechanical properties of cell walls. Lee et al. (2007b) investigated the interphase properties in a cellulose fiber-reinforced polypropylene composite with a continuous stiffness technique. A line of indents was produced from the fiber to the matrix. There was a gradient of hardness and modulus across the interphase region. The distinct properties of the transition zone were revealed by one to four indents, depending on the nanoindentation depth and spacing. It was assumed that the width of the property transition zone is less than 1 micrometer.

Zickler et al. (2006) studied the changes of mechanical properties in pyrolysed spruce wood as a function of temperature up to 2400℃. The results showed that the hardness values increase continuously by more than one order of magnitude to 4.5 GPa at 700℃. The indentation modulus shows complex changes with a minimum of 5 GPa around 400℃ and a maximum of 40 GPa around 1000℃. He hypothesized the deformation introduced by nanoindentation was visco-plastic in wood and purely elastic in the carbonaceous residue.

Another interesting area of research is relate to the effects of thermo-mechanical refining pressure on the mechanical properties and nano- or micro-level damages to the wood cell wall. Xing et al. (2007) found that the cross sectional dimension of fibers subjected to lower pressures was more stable than for fibers subjected to higher pressures. There was no obvious damage in the cell walls at pressures between 2 and 4 bar. Nano-

cracks (most less than 500 nm in width) were found in fibers at pressures in the range of 6–12 bar, and micro-cracks (more than 5 micrometers in width) were found in fibers subjected to pressures of 14 and 18 bar. Xing et al. (2008) also found that refining pressure played an important role on the physical damage of refined wood fibers. In the same refining pressure conditions, the elastic modulus, hardness and creep resistance of the mature fibers were higher than that of the juvenile fibers. When refining pressure increased, the overall trends of elastic modulus and hardness decreased while nanoindentaion creep increased.

The previous research indicates that the mechanical properties such as modulus and hardness of wood cell wall can be measured through the nanoindentation test. Other mechanical properties such as yield stress and compression strength have not been studied.

2.4. Focused ion beam (FIB)

FIB is a powerful tool for the inspection of micro-system. A typical FIB consists of the ion column, the work chamber, the vacuum system, the gas system, and the workstation (Reyntjens and Puers 2001). FIB technology started in 1974, using the gallium liquid metal ion source (LMIS) for sample preparation. Originally several liquid sources, such as cesium, gallium and mercury were used. It was found that the gallium was the most suited liquid (Matsui and Ochiai 1996) because of its long lifetime (over 500 h) and high stability variation (less than ±1%). The typical accelerating voltage is

between 5 and 50 keV while the primary ion penetration depth is ~20 nm at 25 ekV (Giannuzzi and Stevie 1999).

FIB technology was initially used for maskless implantation and lithography instruments (Sugiyama and Sigesato 2004). Afterwards the FIB became a powerful tool in the semiconductor industry for failure analysis and transmission electron microscopy (TEM) specimen preparation (Rubanov and Munroe 2004). There are at least two methods reported for TEM sample preparation which were the cross-section method (Giannuzzi and Stevie 1999) and lift-out technique (Giannuzzi et al., 1998; Stevie et al., 2001; Lanford and Clinton 2004). A method for *in-situ* TEM specimen preparation was also developed (Field and Papin 2004).

Although the most popular application area of FIB is the semiconductor field, FIB is versatile piece of equipment. It can mill many kinds of materials and be used in solid state devices for lithography, etching, deposition and doping (Matsui and Ochiai 1996). Phaneuf (1999) reviewed the FIB applications in traditional material science, including specimen preparation and microscopy inspection. Gasser (2004) researched metal matrix composites prepared by FIB.

References show that recently FIB technology has been applied in earth sciences, aerosol science, pharmaceutical characterization, etc. (Heaney et al., 2001; Kaegi and Gasser, 2004; Moghadam et al., 2006). It is worth mentioning that the FIB technique has been used in the biological material area too. Ishitani (1995) applied FIB for identifying

damageable biological specimens of human hair and the housefly eye. Different kinds of cells were prepared by FIB too (Kamino et al., 2004; Drobne et al., 2005; Marko et al., 2007). Only one reference (Orso et al. 2006) described the FIB application in wood material where cantilevers were fabricated by FIB.

It was reported that at 30 keV, the top 25 nm of a silicon substrate will be amorphized. It should be noted that there will be damage in the sample surface due to heating from the high energy gallium ion beam during milling, although the true extent of damage is unknown (Walker and Broom 1997).

Different methods have been found to reduce the specimen surface damage. Minimizing the milling time may prevent surface heating. It has also been reported that lowering the gallium ion energy in the final step of milling played an important role in reducing the surface damage. Another effective way to remove the surface damage in TEM samples is plasma cleaner (Hata et al. 2006). Low energy Ar ions were induced by immersing the sample in the plasma source, with the $Ar:O_2$ ratio of 3:1. The shallow surface inter-mixing of Ga is then efficiently removed (Ko et al. 2007). Some researchers said the results obtained from a wide range of materials indicated that important results can be obtained without damage layer removal (Matsui and Ochiai 1996). As a result, FIB is powerful equipment for sample preparation and it has already been confirmed that wood material can be milled by FIB.

2.5. Micropillar compression test

Several recently published references have been found relevant to micropillar compression test, especially in the metal composite material area. This novel experiment can avoid strain gradient which happened in the nanoindentation test (Swadener et al. 2002), and other mechanical properties, like the yield stress, can be explored.

First of all, there are some requirements of the micropillar for the compression test. Zhang et al. (2006) designed an accurate model for micro-compression testing. In this model, they suggested that the post aspect ratio (defined as height/diameter ratio) should be less than five, the fillet radius /post radius ratios should be between 0.2 and 0.5. Taper of the post and misalignment of the micro-compression system should be avoided because this shape may generate higher mechanical properties which are not reasonable.

Many micro compression tests were performed to investigate the "size effect" which was that the mechanical properties would increase while the diameter decrease into micro or nano scale. Uchic and Dimiduk (2005) first develop this uniaxial compression testing on micropillar to investigate the size scale effects. They introduced the FIB system for sample preparation. The Ni super alloy was milled by FIB into cylindrical shape, then compressed by a nanoindentation device with a flat tip. Throughout the experiment, the size effect was observed at the size of five and two micrometers in diameter. Volkert and Lilleodden (2006) performed compression test on micron and sub-micron single crystal Au columns prepared by FIB. They found that both the yield stress

and apparent strain hardening rate increased strongly with decreasing column diameter. Moser et al. (2007) did *in-situ* SEM micro-compression test on Si micropillars. They used the plasma Alcatel 601 etcher to mill the pillars. The results showed that the small diameter pillars tend to buckle while larger ones tend to crack. They also discovered that the compressive strength increased with decreasing pillar diameter.

Greer et al. (2005) conducted uniaxial compression tests on single-crystalline <0 0 1>- oriented gold pillars of diameters between 300 and 7450 nm milled by FIB. The pillar yielded at stresses much higher than the one of bulk gold of ~ 30 MPa at two percent strain.

Bei et al. (2007) used the chemically etching method to mill the single-crystal micropillar of a molybdenum alloy, and then compressed them with a nanoindentation system. The pillars yielded at a critical resolved shear stress of 4.3 GPa which was in the range expected for the theoretical strength. The effects of FIB milling on the mechanical behavior was also investigated by Bei and Shim (2007). They found that the FIB milling may introduced damage that obviates the need for dislocation nucleation during subsequent deformation.

Michler et al. (2007) investigated the compressive strength of gallium arsenide (GaAs) milled by FIB, finding the yield stress to be 1.8±0.4 GPa. Another interesting phenomenon was that the micropillars exhibited ductile plasticity compared to macroscopic tests.

2.6. Summary

The physical and mechanical properties of commercially important wood species have well been studied and documented. This is highlighted by authoritative wood science references such as Wood handbook (1999), the Encyclopedia of Wood (1989) and ASTM D2555 (Standard Practice for Establishing Clear Wood Strength Values) that list the important mechanical properties of the representative wood species in North America.

Nanoindentation is a useful tool for testing the mechanical properties of individual wood cell walls, such as longitudinal hardness and modulus of elasticity (MOE). However, these properties may be influenced by plastic strain gradients imposed during the testing (Swadener et al. 2002). Other important properties of the wood cell wall such as yield stress and compression strength are still remained undiscovered yet. This creats an opportunity for new methods to be developed for discovering other mechanical properties of wood cell wall.

The FIB system is powerful equipment. It has already been used to mill wood specimens. As related to micropillar compression testing, much research has been done. However, there is an absence in the literature of the micropillar compression test of the wood cell wall.

CHAPTER 3 MATERIALS AND EXPERIMENTAL PROCEDURE

3.1. Materials

Given the objectives of the thesis, one species of hardwood and one species of softwood were chosen to be used for the uniaxial micropillar compression test. The two samples were chosen from ten existing lab specimens. First, the non-contact mode of AFM was used to check the thickness of these wood cell walls (Figure 3-1). The variation of the thickness was extremely significant among all the species, ranging from less than one micrometer to approximately ten micrometers. Figure 3-2 was a typical AFM topography of loblolly pine, the arrowhead shows the thickness of the wood cell wall.

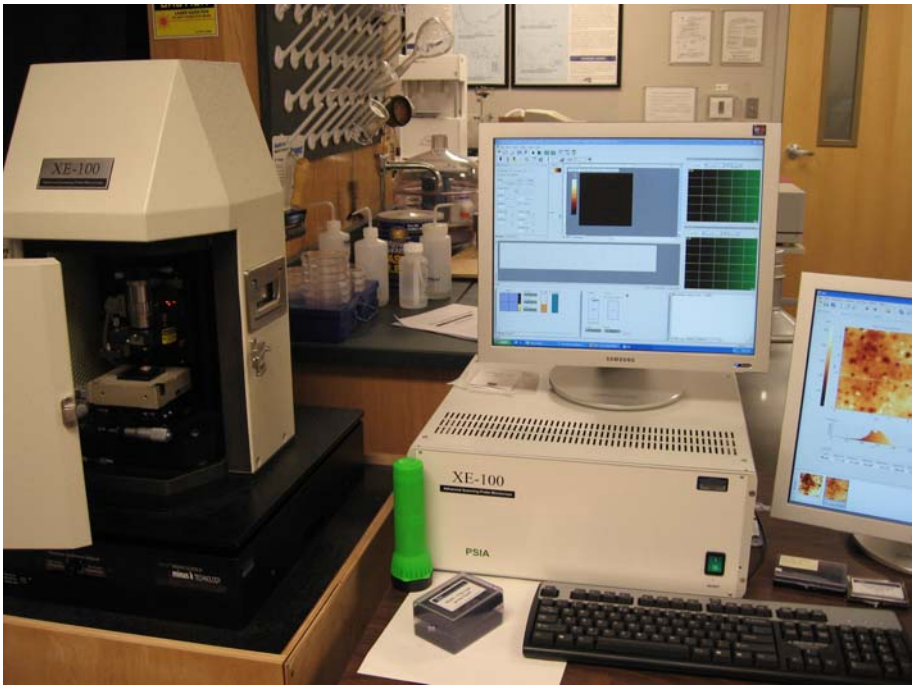

Figure 3-1. Atomic Force Microscope (AFM)

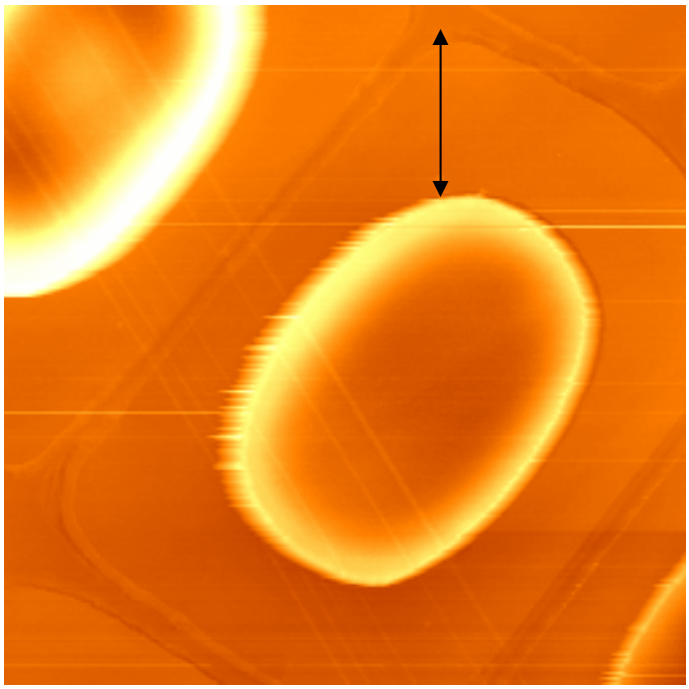

Figure 3-2. A typical AFM image of loblolly pine cell wall

The thickness of the wood cell wall should be large enough to make sure that there is enough space to mill micropillar. The thicker the cell wall, the better the sample preparation. Finally, two kinds of wood species with the large thickness of cell wall were chosen. One representative of softwood is loblolly pine (*Pinus taeda*) and the hardwood species is Keranji (*Tectona*).

Loblolly pine (*Pinus taeda*) is one of several pines native to the southeastern United States, used mainly as the raw material for Oriented Strand Board (OSB) and structural lumber. Keranji (*Tectona*) is native to Southeastern Asia. It is widely used as flooring material for interior decoration.

3.2. Sample preparation

The sample preparation process included two steps. First, microtome was used to flatten the surface of the sample (the sample for nanoindentation test should be embedded in the epoxy resin before microtome), Second, FIB milling was used to fabricate one micropillar in a single cell wall.

3.2.1. Initial sample preparation

First, the micro-sample fabrication process began with the preparation of the bulk material of interest. Both samples of softwood and hardwood were cut from one single growth ring. Next the earlywood part of the sample was removed. The latewood part was cut into 3mm×3mm×2mm dimensions by a blade initially.

Second, one of the transverse (cross-sectional) surfaces was glued to an acrylic block by a five-minute epoxy. The acrylic block was mounted on a microtome, another transverse surface of the sample was cut by a blade under an optical microscope. When that surface was flat inspected by the microscope, the sample was separated from the acrylic block, the flat surface was glued to the acrylic block. The opposite surface was cut by the blade under an optical microscope, as well.

Lastly, the acrylic block was transferred to the ultra-microtome (Figure 3-3). The sample was leveled cross-sectionally and transverse-sectionally with a glass knife. Finally the surface would be smoothed using a diamond knife. After the microtoming, the shape

of the sample was trapezoidal (Figure 3-4). The ideal dimension was 1.5mm in length, 1mm in width and 0.5mm in thickness.

3.2.2. Dimension determination of micropillar

Before FIB milling, some parameters of micropillar should be ascertained. Figure 3-5 shows an ideal simulated micropillar for compression test. The diameter of micropillar should be smaller than the thickness of the cell wall to ensure that a micropillar is generated in a single cell wall. Based on the thickness condition of loblolly pine and keranji, the diameter of micropillars was chosen from five to eight micrometers.

Figure 3-3. Process of microtoming

Figure 3-4. Loblolly pine cell wall after ultra-microtoming under optical microscope

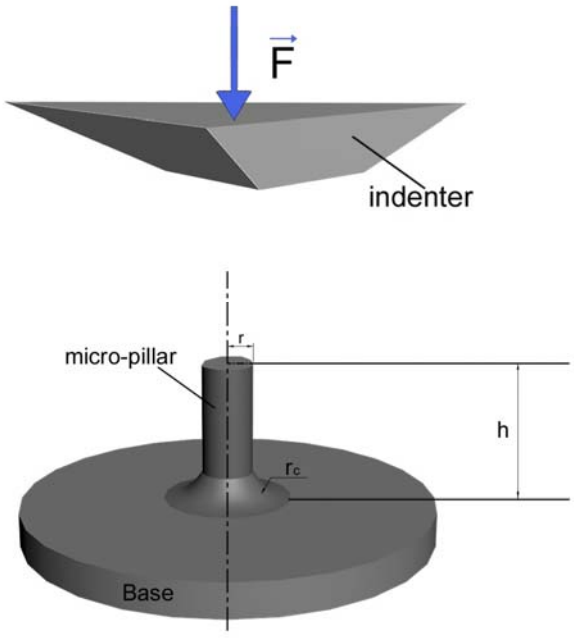

Figure 3-5. Model of micropillar for compression test

The pillar aspect ratio, defined as the height/diameter ratio, is an important parameter of pillar for micro compression test. Aspect ratio should be less than five (Zhang et al. 2006), or the pillar can not be compressed correctly and it may prematurely buckled during the test.

3.2.3. FIB milling

The FIB milling used highly localized ion sputtering using energetic ions to micro-machine small compression samples into the surface of the bulk material. When the sample was put into the FIB chamber, the surface of the bulk section was oriented normal to the FIB column and the exact wood cell wall area of interest was then located by FIB imaging.

In a typical area, a concentric annular milling pattern was used to mill a cavity. The specific parameters to mill the micropillar is given in Table 3-1. The diameter of the inner circle was exactly the same as the micropillar diameter, the diameter of the outer circle was 30 micrometers. Any material between the inner circle and outer circle of this concentric annular milling pattern is etched to a certain depth by the ion beam. Because of the highly energized ion beam, the actual diameter of micropillar should be smaller than the target.

Figures 3-6 illustrates the FIB system (FB 2000A, Hitachi, Japan) which was used to mill the wood specimen. Because this FIB is a time-controlled machine, the length of the micropillar could not be milled to the exact target directly. So several micropillars

were milled at first in trial, each micropillar was milled a certain numbers of times (such as 30 minutes, 60 minutes, 90 minutes and so on), then the gage length of these micropillars were measured. Approximate relationships between the FIB milling time and the length of micropillar was obtained. When the formal FIB milling was conducted, each micropillar was milled for about 75 minutes.

There were specific reasons to mill the large outer circle, where the diameter was 30 micrometers. First, this large cavity allowed the Nano II indenter system used to do the micro compression test, to easily locate the micropillar position. This was important because it was difficult to find these micropillars inside hundreds of wood cells of the complete specimen. This was confirmed by the following compression test. Under the optical microscope of the Nano II indenter system, these micropillars were discovered clearly because of the large outer cavity.

Table 3-1. Parameters for operating FIB system

Beam voltage (KeV)	Beam current (nA)	Extraction voltage (KV)	Aperture	Emission current (KV)
30	7.617	6.33	MI-300	2.4

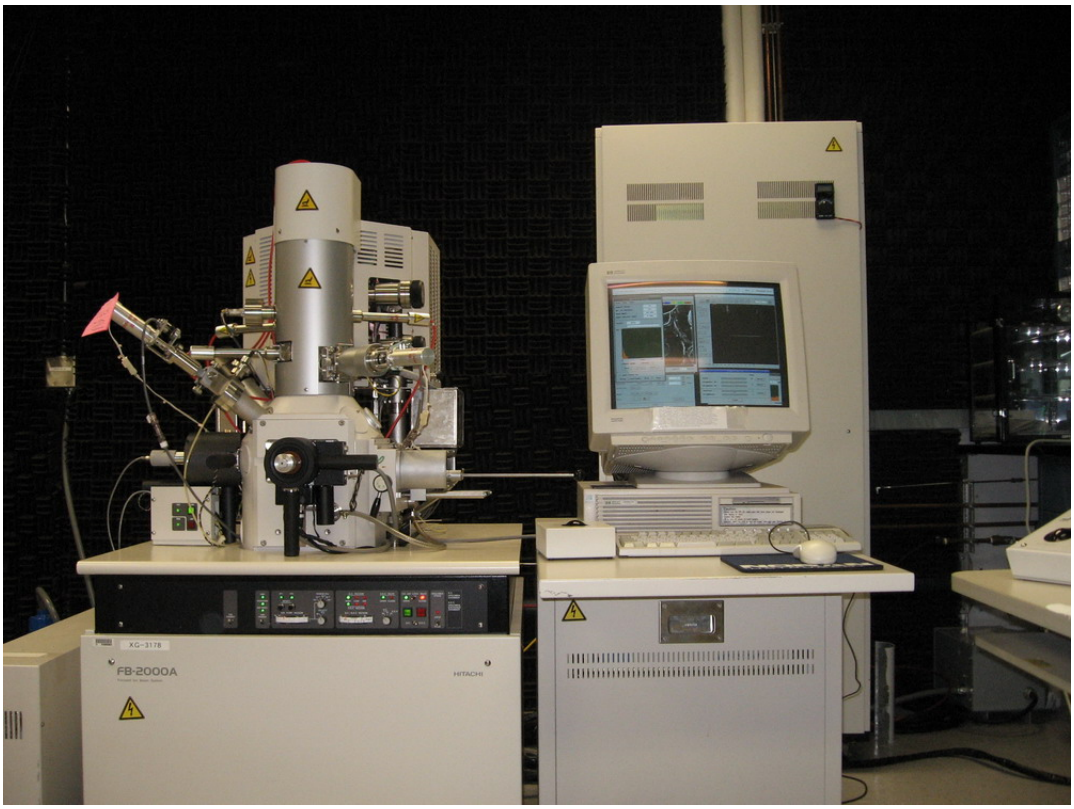

Figure 3-6. Focused Ion Beam System (FIB)

Secondly, the outer circle should be large enough to make sure the edge of the flat indenter tip did not touch the outside wood cell walls other than the micropillar, which would strongly influence the accuracy of data.

Third, it made the empty space large enough, so the SEM images could clearly detect the sidewalls of the micropillar both before and after the compression test. This made it easy to measure the dimension of the micropillar. Another square in addition to the outer circle was milled in hardwood sample to make sure that the sidewall of the micropillar could be clearly identified.

When the FIB milling was completed, the sample was taken out of the FIB chamber and attached on a standard scanning electron microscope (SEM) stub by the carbon tape (Figure 3-7). This SEM stub could be fit into both the stages of the SEM and Nano II Indenter system, which were used for imaging and performing the micro compression test respectively. The sample was then put under the condition of 22.2℃ (temperature) and 38% (relative humidity) for 2 weeks. These conditions were the same as the conditions in the room where Nano II Indenter system was placed. After that, the sample was stored in a sealed case which is typically used to store an electron microscope specimen.

Figure 3-7. SEM stub and sample storage box

3.3. Scanning electron microscope (SEM)

The SEM used in this project was a LEO 1525 (Zeiss Instruments, USA) shown in Figure 3-8. In the SEM system, an electron source emitted electrons under the influence of a current. The electron beam was focused on the sample in a vacuum chamber using rotational electromagnets. The electrons that stroke the surface of the specimen generate secondary electrons from the specimen surface. These secondary electrons have a low energy and can not escape from a depth greater than 10 nm.

Secondary electrons were detected by secondary electron detectors, which amplified and changed the signal to an electric one. A three-dimensional image was constructed from the number of electrons emitted from different spots on the sample at a resolution around one to five nm.

Figure 3-8. SEM system

The SEM system played an important role in this whole experiment and provided information about the topography of a specimen. The images of the same micropillar were taken both before and after the compression test in order to evaluate whether the data received from this micropillar was reliable.

When the sample was put into the SEM chamber, the stage was lowered (the working distance was approximately 26 mm) and the magnification was decreased to find the specimen. The stage was then moved up to allow for a working distance of approximately six mm. This position allowed for high resolution images. The magnification and focus was changed correspondingly.

The parameter of SEM to take a picture was as follows:

Beam energy	5-10 KV
Working distance	6 mm
Aperture	60 mm

Another important application of SEM images was that it was used to measure the dimensions of the micropillar. Prior to testing, SEM images were taken at tilt angles of 36 degree and a scale was attached to the image. ImageJ software was used to analyze these images. The diameter and the length of micropillar was then measured.

3.4. Micropillar compression test

The micropillar compression test was performed in a Nano II Indenter system using a flat punch (Figure 3-9). The punch is a 60° conical indenter that has been truncated to form a ten micrometers diameter circular flat surface.

As mentioned before, after sample preparation, the sample was glued to the SEM stub. This stub could be fit into the Nano II system stage (Figure 3-10) to be sure that the sample surface would be vertical to the flat punch, which was very important to obtain the correct data.

Figure 3-11 shows the inside Nano II Indenter system. The optical microscope is on the right, magnification ranging from 500 to 1500, with the indenter punch located on the left.

The stage with the sample could be moved in X and Y directions horizontally between the microscope and the indenter punch. It could also be moved up and down to let the indenter contact the specimen surface.

The optical microscope was used to locate the position of the micropillar. Once a micropillar was found under microscope, calibration was performed at first. A place near that micropillar was chosen under the microscope and the sample was then moved to the indenter punch for the indenter. After that, the sample was moved back under the

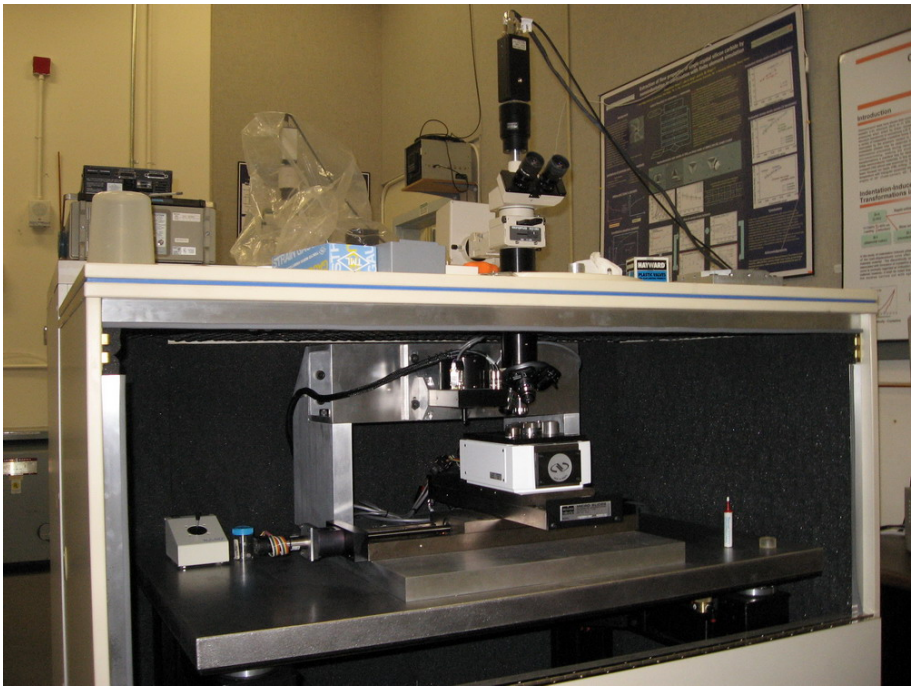

Figure 3-9. Nano II Indenter system

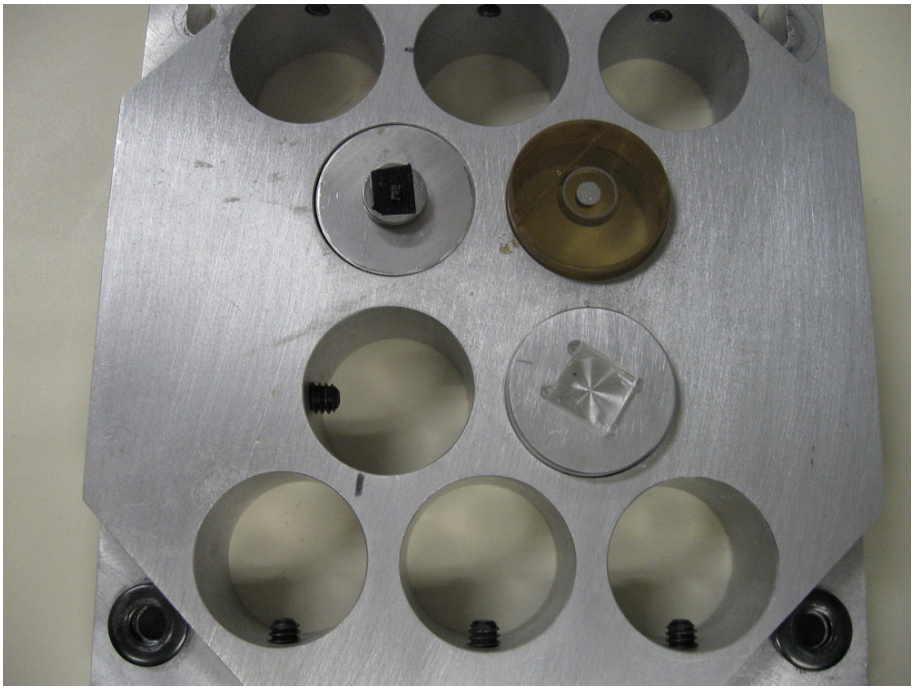

Figure 3-10. Sample stage of Nano II Indenter system

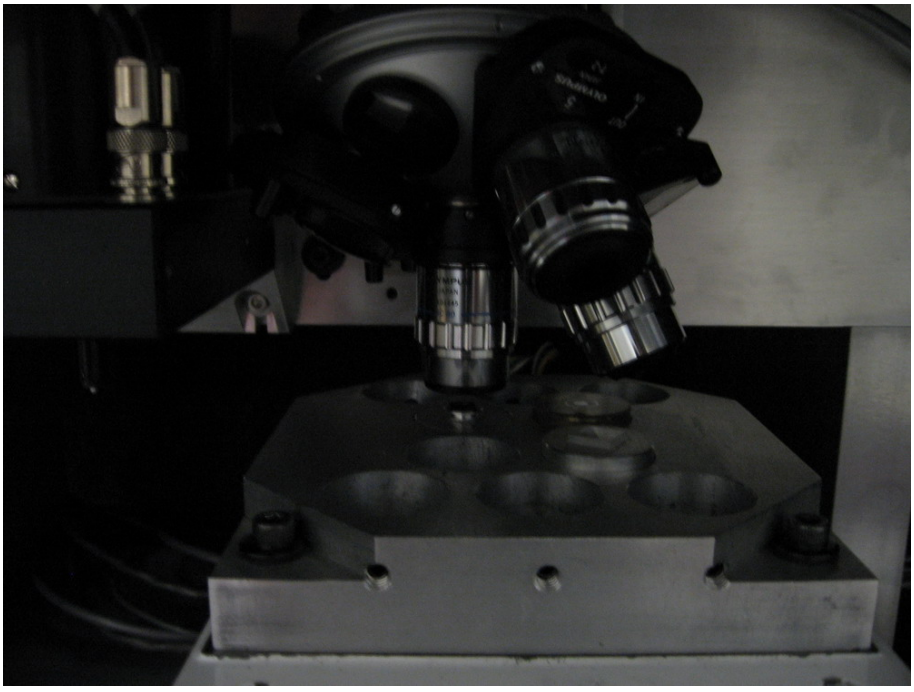

Figure 3-11. Inside Nano II Indenter system

microscope. If the cross in the microscope was not in the same place as the indentation, the adjustment was done by moving the cross to the place of indentation and was recorded by the machine. This is the process of calibration. An important point is that this calibration was done for every single micropillar before a compression test, to make sure that the punch would compress the pillar in the ideal location.

The temperature and relative humidity in the test room was constantly 22.2℃ and 38%. The procedure of the whole compression test consisted of three segments which are as follows:

- loading, when the tip touched the surface of micropillar, the loading rate was 20 nm/s, compression depth was between 1 to 3 micrometers;

- holding, the holding time was 1 s;
- unloading, the rate was the same as the loading rate.

In this procedure, the loading process was the most important (also known as "approach segment"). The purpose of the approach segment was to determine accurately the "zero" of the compression punch (i.e., the values of punch load and displacement at the point where the tip of the punch just touched the surface of the pillar). These values were obtained as follows.

The position of a micropillar was selected under the microscope. When the compression test began, the whole specimen was moved under the tip to a point 50 micrometers away from the micropillar location. The Z-stage moved the sample up for the first surface finding indent, and then backed the sample away. The sample was then moved half of the offset distance (25 micrometers), and the Z-stage again drove the specimen up for the second surface find. The Z-drive did not move from this point until the next surface was found. Finally, the sample was moved to the position of the micropillar indent and the experiment began.

After the compression test, the load and displacement data would be generated. The conversion of the load and displacement data from the nanoindenter to a stress–strain curve was a straightforward process, and was analogous to calculate a stress–strain curve for a macroscopic compression sample. The formula used for calculation was as follows:

Strain (ε) can be calculated from equation 4,

$$\varepsilon = \frac{\Delta l}{l_0} = \frac{l_0 - l}{l_0} \tag{4}$$

Where the l_0 is the original length of micropillar, l is the length of micropillar after compression test, Δl is the deformation under testing.

Stress (σ) can be calculated from equation 5,

$$\sigma = \frac{P}{A} = \frac{P}{\frac{1}{4}\pi d^2} \tag{5}$$

Where P is the measured force on the micropillar, A is the area of cross section of micropillar, d is the diameter of micropillar.

To measure the engineering modulus (E), continues compression testing was performed on some micropillars. The procedure was almost the same as the former one, but the compression depth was 200 nm for the first loading, 400 nm for the second loading and 600 nm for the third loading. The exact procedure was as follows:

Cycle 1:

- loading, while the loading rate was 20 nm/s, compression depth was 200 nm;
- holding, the holding time was 1 s;
- unloading, the rate was the same as the loading rate.

Cycle 2 and Cycle 3 was almost the same as cycle, but the compression depth for each time was 400 nm and 600 nm.

E is the slope of elastic part of the stress-strain curve and it can then be calculated from equation 6,

$$E = \frac{\sigma}{\varepsilon} \tag{6}$$

3.5. Nanoindentation test

The nanoindentation test was performed on the samples of same species which were keranji and loblolly pine. The sample preparation was similar to the initial sample preparation for micro-compression test, the only difference being that the sample for nanoindentation test was embedded in epoxy resin first, and then the microtome was performed.

The finished sample was arranged in a silicon mould and soaked in Spur epoxy resin (Spur 1969). Table 3-2 shows the component of epoxy resin. The embedded sample was put in a desiccator and under vacuum for overnight to remove air bubbles. The sample position was such that the cross-sectional surface is uptilt. On the next day, the resin-impregnated sample was removed from the desiccator and transferred to a flat mould, then fresh prepared epoxy resin was filled in. The mould containing both wood samples and epoxy resin are then placed in an oven at 70℃ for 12 hours.

Table 3-2. Component of Spur epoxy resin

Name	ERL-4221	DER-736	NSA	DAME
proportion	5	3	13	0.2
weight	2.5g	1.5g	6.5g	0.1g

Figure 3-12 shows a typical load-displacement curve of nanoindentation test. The procedure for nanoindentation test was as follows: loading rate was 2 nm/s, the indentation depth was 150 nm, holding time was 20 s, then unloading with rate of 10 nm/s to 90%, then hold for 60 seconds, finally completely unload.

After test, Oliver and Pharr method was used to calculate the modulus and hardness (Oliver and Pharr 1992). In the test, the hardness (H) of the samples for an indentation depth (h) was calculated as:

$$H = \frac{P_{\max}}{A} \tag{1}$$

where P_{max} is the load measured at a maximum depth of penetration (h) in an indentation cycle, and A is the projected area of contact between the indenter and sample at P_{max}.

The combined modulus of the system, or reduced indentation modulus (E_r) was determined as:

$$E_r = \frac{dP}{dh}\frac{1}{2}\frac{\sqrt{\pi}}{\sqrt{A}} \tag{2}$$

where $\frac{dp}{dh}$ is the slope of the line tangent to the initial unloading curve in the load–displacement plot.

The sample modulus (E_s) was then be calculated as:

$$E_s = (1 - \nu^2{}_s)(\frac{1}{E_r} - \frac{1 - \nu_i{}^2}{E_i})^{-1} \quad (3)$$

where ν_s and ν_i are the Poisson's ratios of the specimen and indenter, respectively, and E_i is the modulus of the indenter.

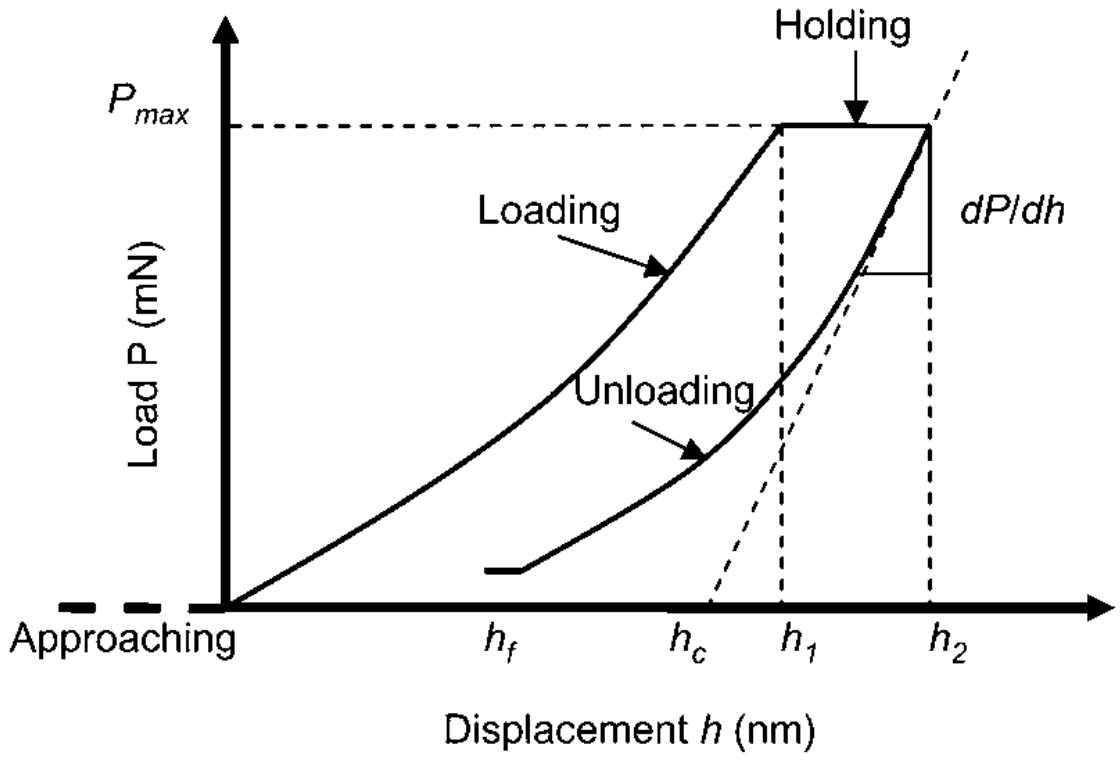

Figure 3-12. A typical load-displacement curve during indentation

CHAPTER 4 RSEULTS AND DISCUSSION

4.1. Quality of wood micropillars

Before uniaxial micro compression testing, every micropillar was evaluated using SEM images. Figures 4-1 and 4-2 show the overview of hardwood and softwood specimen after FIB milling, both images were taken at 36° tilt from horizontal. There are 25 hardwood micropillars and 12 softwood micropillars milled by FIB. From these images, micropillars were easily identified from the empty hole between the micropillar and the nearby cell wall.

Before the micropillar compression test, the SEM image was used to evaluate the quality of the micropillars, which helped to decide whether these micropillars were good enough for a compression test. Images of the micropillars after the compression test were also taken to see whether these pillars were compressed correctly.

Figure 4-3 shows the good micropillars after FIB milling, while (a) was keranji (hardwood) and (b) was loblolly pine (softwood). Micropillars like these had good shape and qualified for the compression test. There are 17 good shaped hardwood micropillars and 8 good shaped softwood micropillars. It was clear that a square shaped hole was milled near the empty outer circle in the hardwood micropillar specimen, which made it easy to check the sidewall of the pillar and measure the length when the specimen was tilted to a certain degree. Because the cell lumen of softwood specimen was much larger

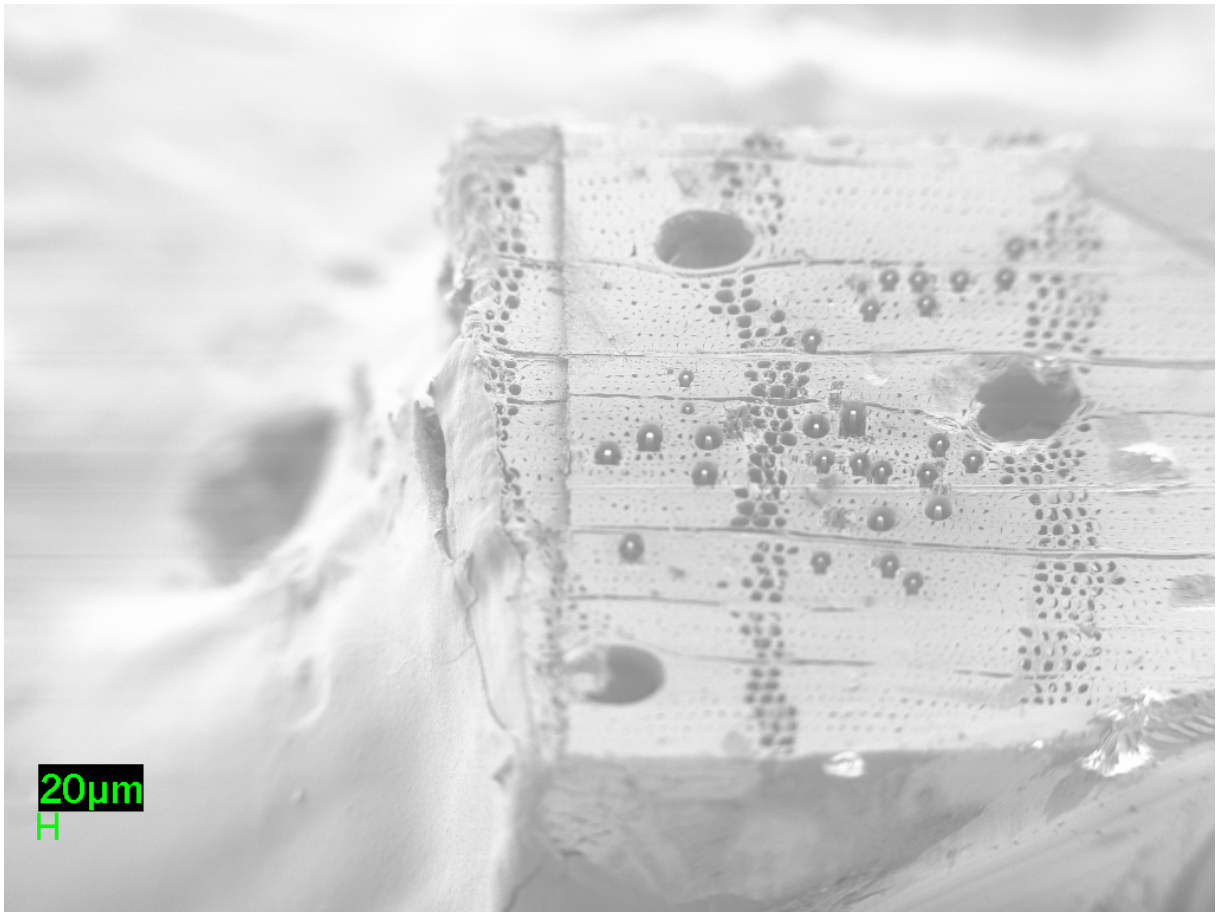

Figure 4-1. SEM image of the hardwood sample after FIB milling at 36° tilt

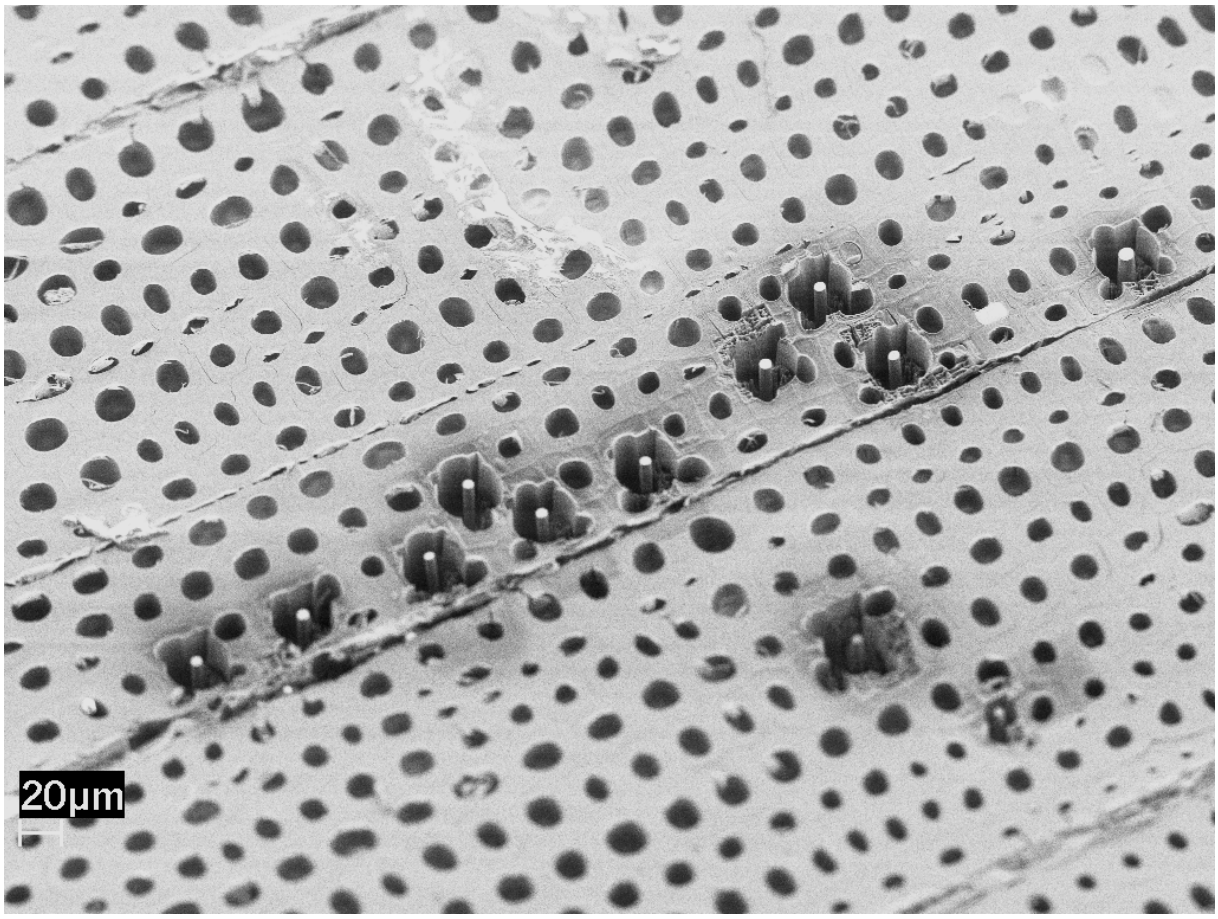

Figure 4-2. SEM image of the softwood sample after FIB milling at 36° tilt

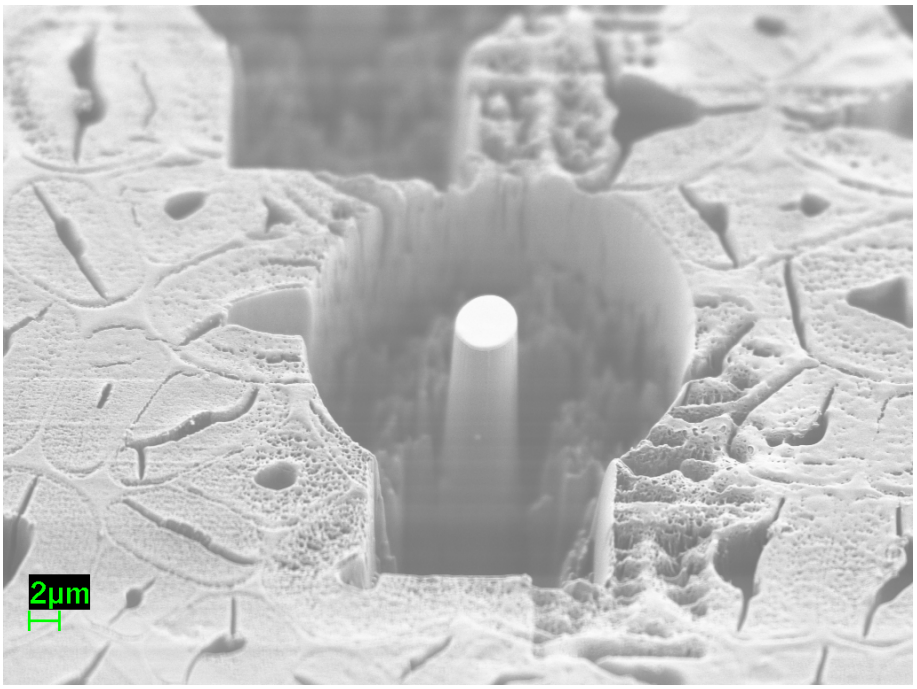

(a)

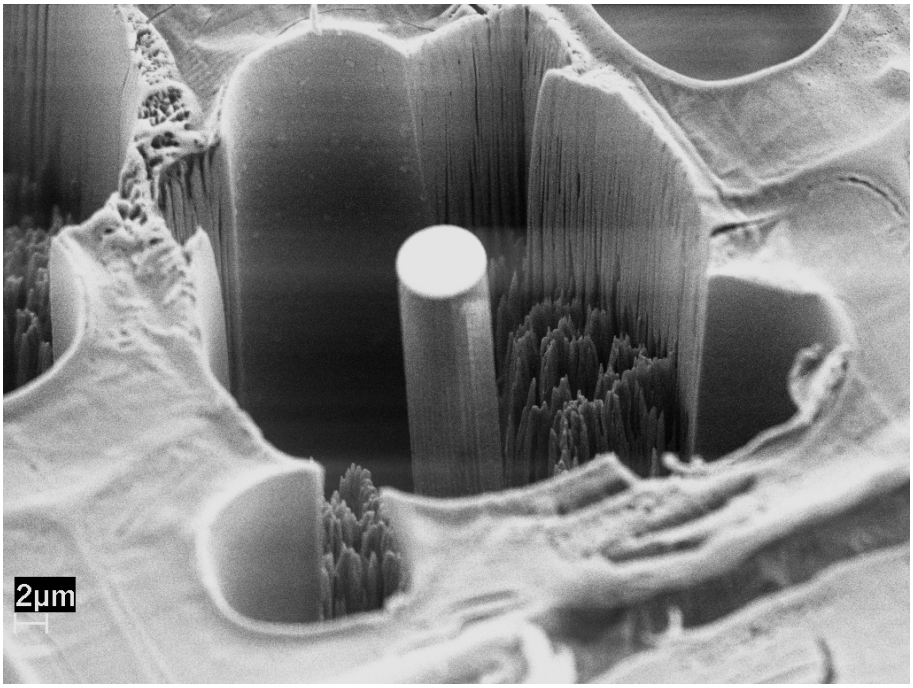

(b)

Figure 4-3. SEM image of representative micropillar after FIB milling at 36° tilt

(a) hardwood micropillar with diameter of 4.75 micrometers
(b) softwood micropillar with diameter of 5.56 micrometers

than the one in hardwood specimen and most of them were of regular round shape. This helped to conveniently check the sidewall. It was not necessary to mill another square near the outer circle and this saved the FIB milling time.

But not all the micropillars were as good as the above ones. Figure 4-4 shows some unqualified micropillars, the one in image (a) was seriously tapered. Another one in image (b) was not milled completely; there were still too many residues attached to the micropillar below the middle height. These pillars were the result of insufficient FIB milling time. Both these kinds of micropillars would generate overestimated mechanical properties, so these type of micropillars were discarded.

4.2. Fracture behavior of wood cell wall

After the initial SEM checking, the micro-compression test was performed on the qualified pillars. To make sure that the data from the test was reliable, the SEM images after compression test were also checked. Figure 4-5 shows a hardwood micropillar (a) before test and (b) after test. It was clear that the compression test was not performed correctly. As a result, this micropillar was buckled. The mechanical properties that came from this pillar test were much lower than the reasonable ones, so data from similar conditions was also discarded.

Normally a material will exhibit the same fracture behavior no matter in bulk form or micro (nano) form. But an exception happened that GaAs micropillars exhibited ductile plasticity contrary to macroscopic tests (Michler et al. 2007).

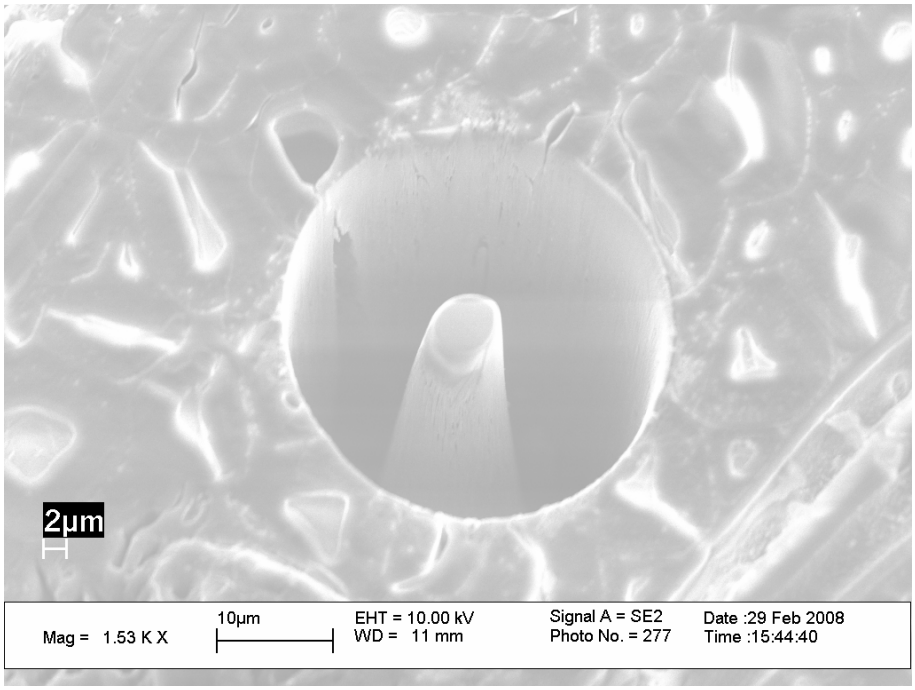

(a)

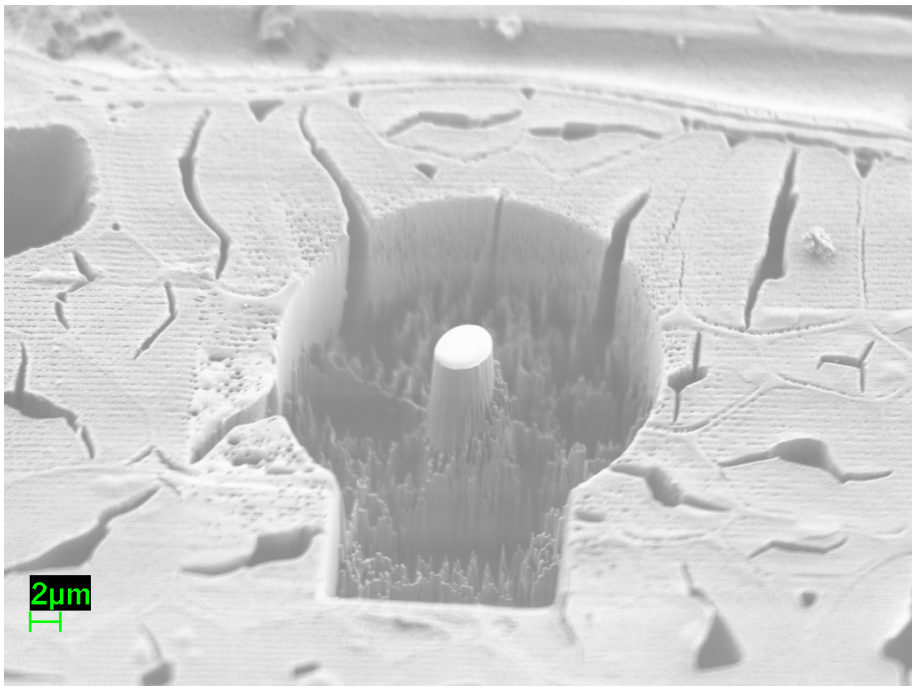

(b)

Figure 4-4. SEM image of the hardwood micropillar at 36° tilt

(a) serious taper shape, (b) FIB milling imperfection

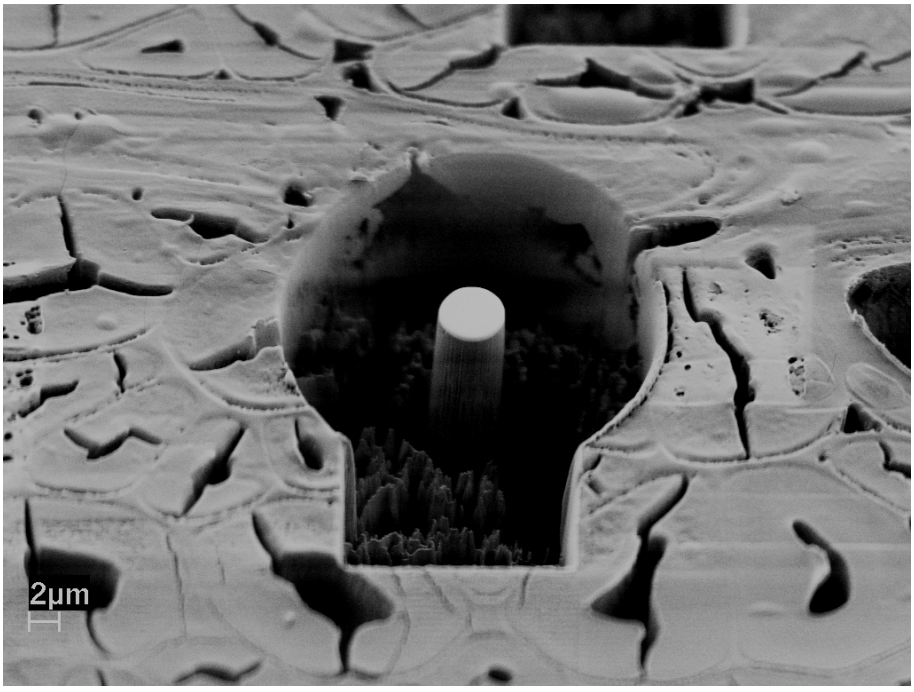

(a)

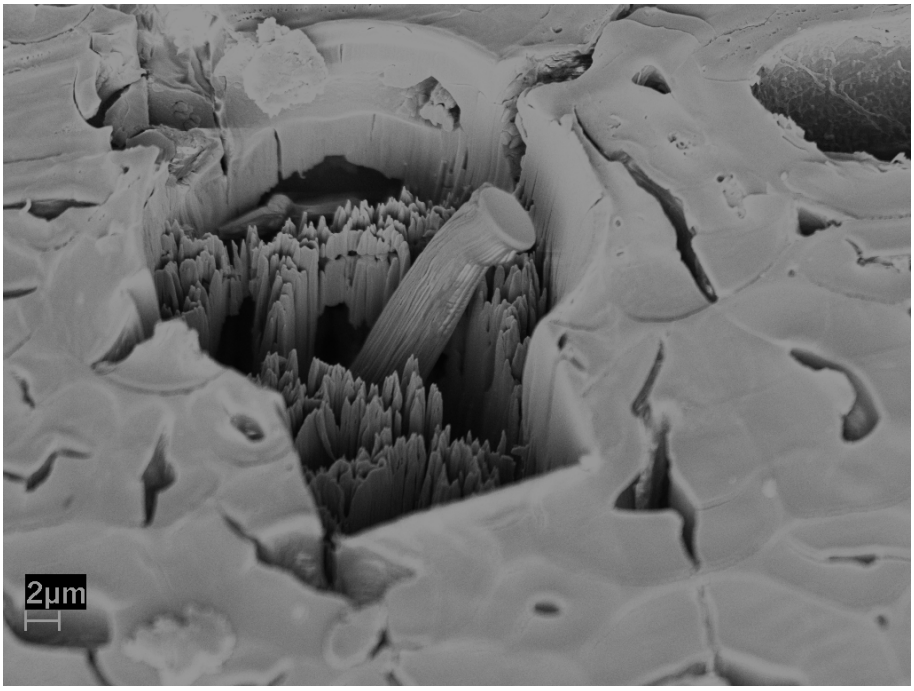

(b)

Figure 4-5. SEM image of the hardwood micropillar with 4.7 micrometers diameter at 36° tilt (a) before testing, (b) after testing

It was confirmed that the bulk wood is brittle material. When compressive load is added to the hardwood timber parallel to grain, visibly well defined patterns of buckling failures will be developed (Koch 1985). In the round specimens, the failure lines come from a single plane (if there is no pith in the specimen) or double helix (if there is pith in the center of the specimen). Figure 4-6 shows the broken spruce wood sample after compression test. The cracks were clear in the sidewalls of the sample, especially in the right amplified image.

In some cases, the compression test was stopped before the micropillar was totally destroyed. These partial compressed pillars provide insight into how the micropillars broke. For example, in Figure 4-7 (b), a small split was generated in the top sidewall of a hardwood micropillar with diameter of 5.75 micrometers during the compression test.

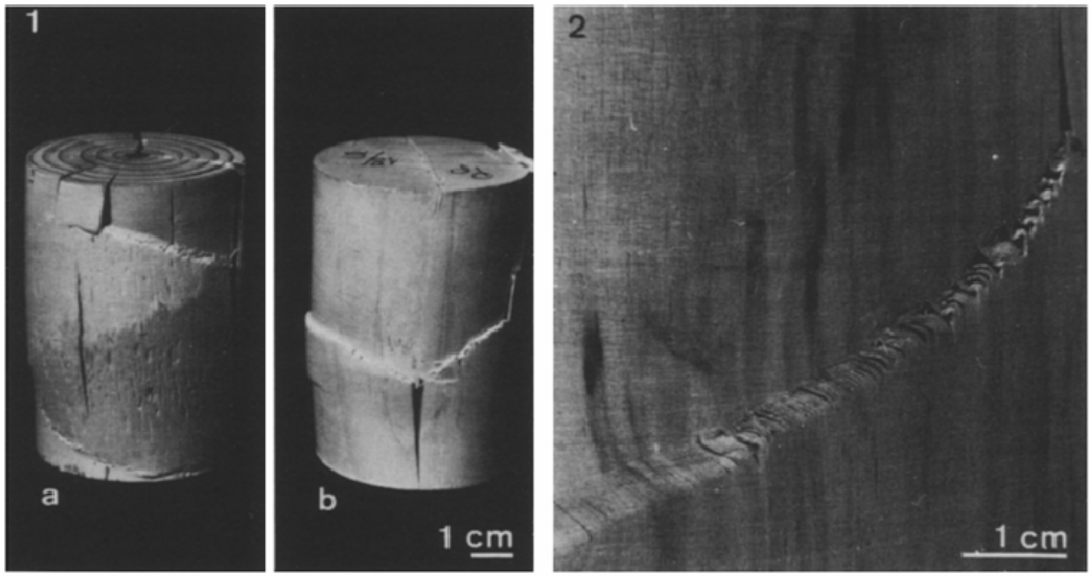

Figure 4-6. Spruce wood sample after compression test (Bariska and Zurich, 1985)

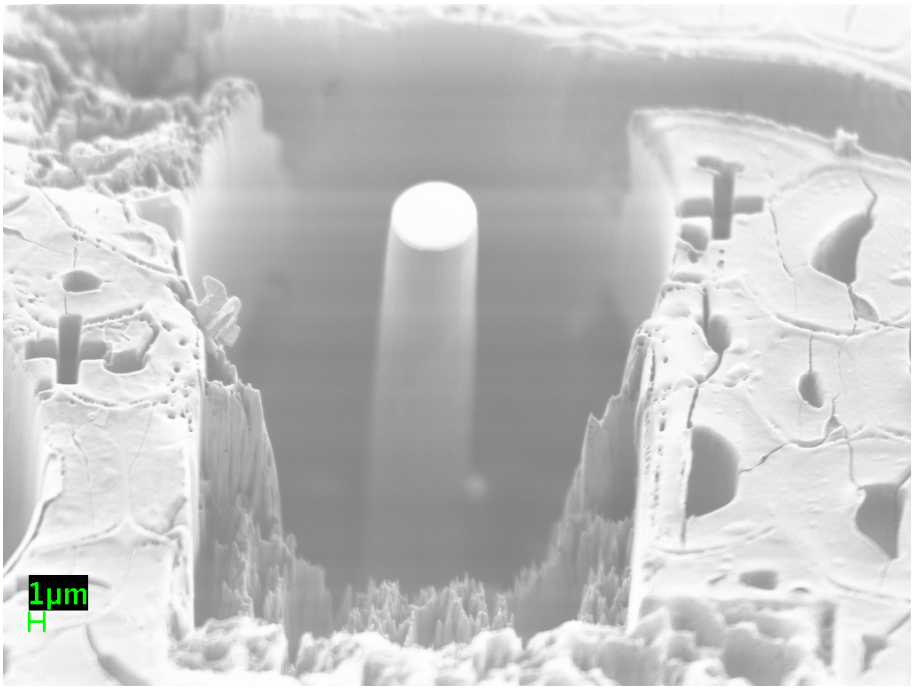

(a)

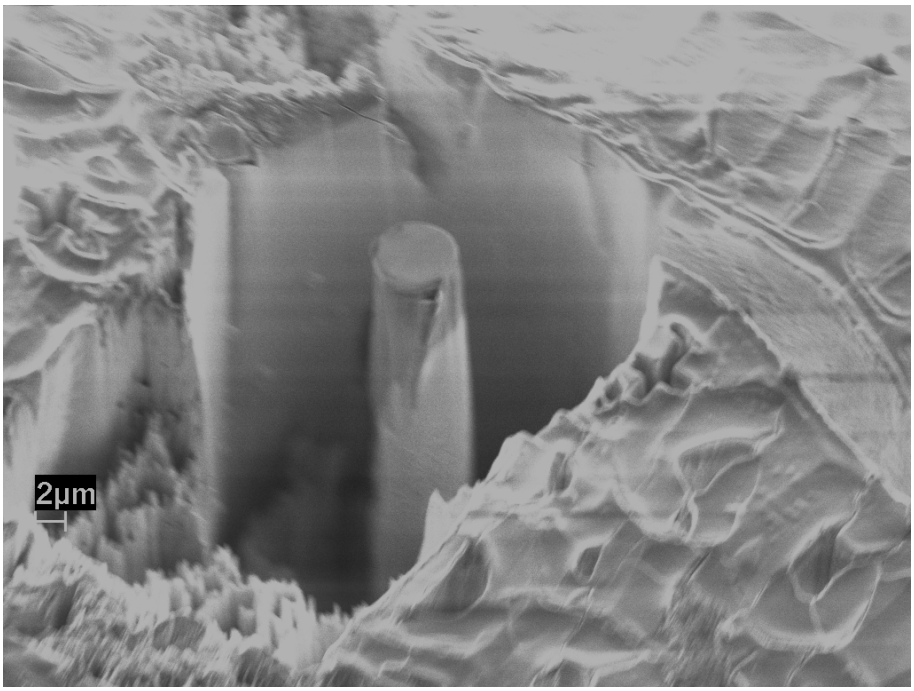

(b)

Figure 4-7. SEM image of the hardwood micropillar with 5.75 micrometers diameter at 36° tilt (a) before testing, (b) after testing

The SEM images from Figure 4-8 to Figure 4-17 show the micropillars before (a) and after (b) compression test. The tilt angle was 36° for both images in all the figures. Among these images, Figure 4-8 to Figure 4-15 were keranji while Figure 4-16 and Figure 4-17 were loblolly pine.

The compression depth of each pillar were different due to the condition of pillar length, normally the compression depth was about 1 micrometer to 3 micrometers. As a result, the micropillars were compressed to different extent, some compression test stopped right after the pillar broke, but some pillars were over-compressed. For the hardwood micropillars, a broken rupture occurred in the sidewall after compression test. In Figure 4-8, many cracks were generated at the top of micropillar after compression test. In some cases, the broken part of the micropillars remained attached to the other part of pillar (Figure 4-12, for example). In other cases, the top was removed completely (Figure 4-9). In Figure 4-11, the broken split even occurred in the middle part of the micropillar as the compression depth was too large and it was over-compressed.

The fracture behavior of softwood micropillars (Figures 4-16 and 4-17) was similar to the one of hardwood micropillar. There was an obvious shift between the top and rest part of the micropillar and cracks could be observed clearly on the sidewall surface of the compressed micropillar. From these images, it was found that most of the cracks happened near the upper top at about 10% of the height of the pillar.

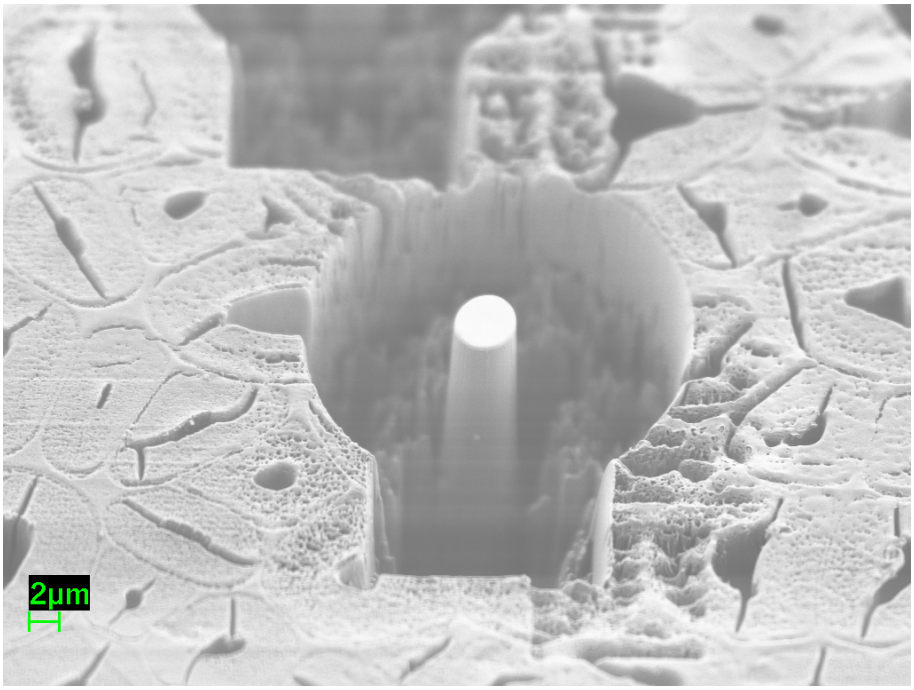

(a)

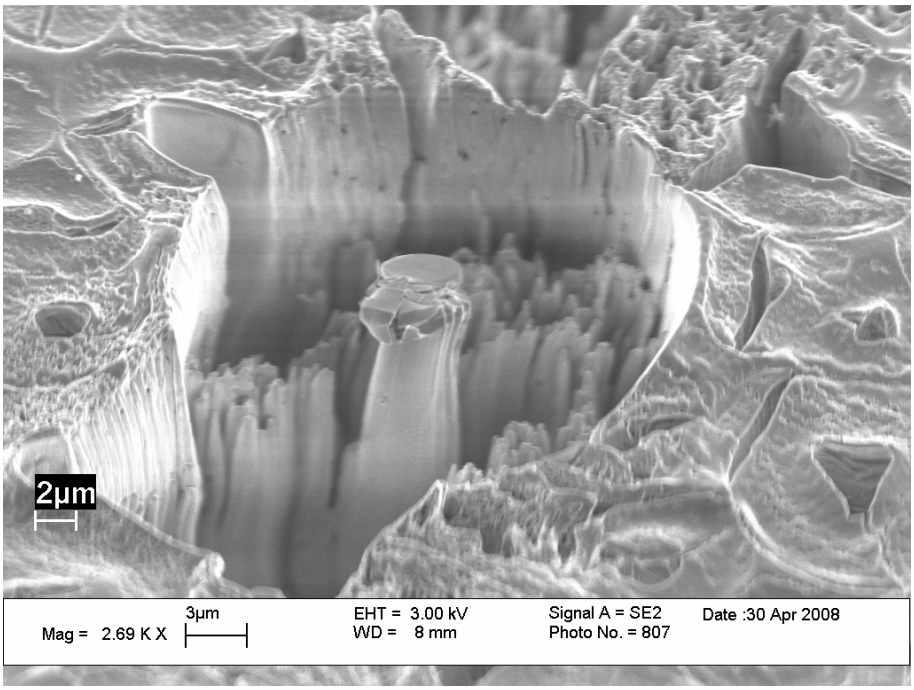

(b)

Figure 4-8. SEM image of the hardwood micropillar with 4.75 micrometers diameter at 36° tilt (a) before testing, (b) after testing

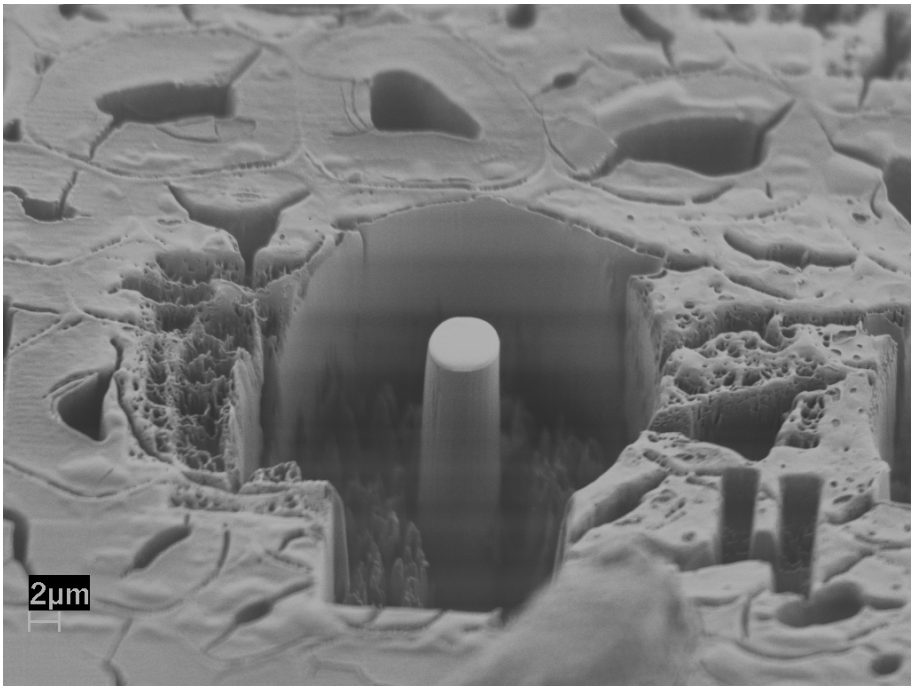

(a)

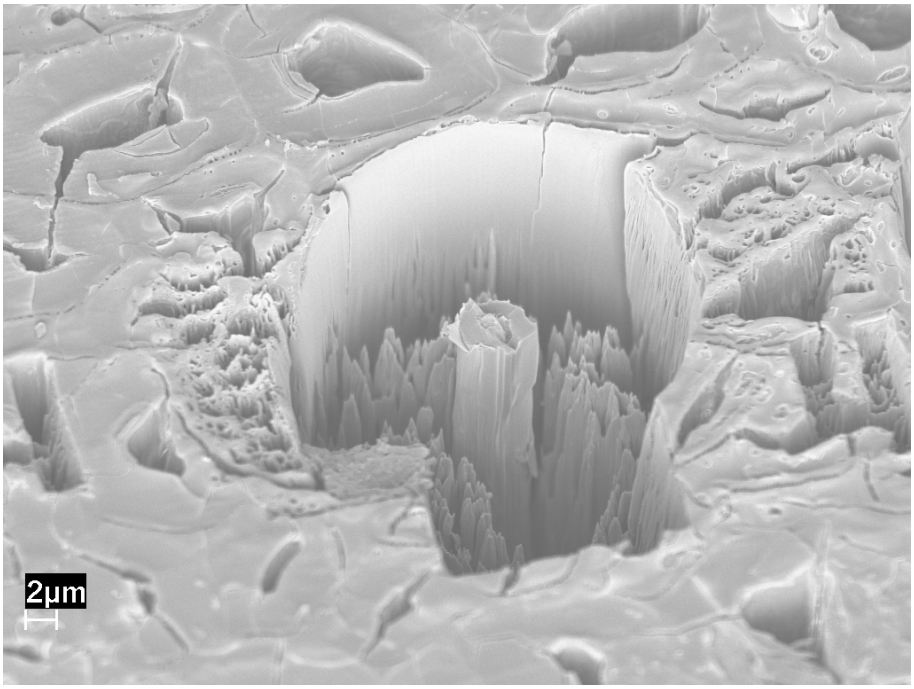

(b)

Figure 4-9. SEM image of the hardwood micropillar with 4.6 micrometers diameter at 36° tilt (a) before testing, (b) after testing

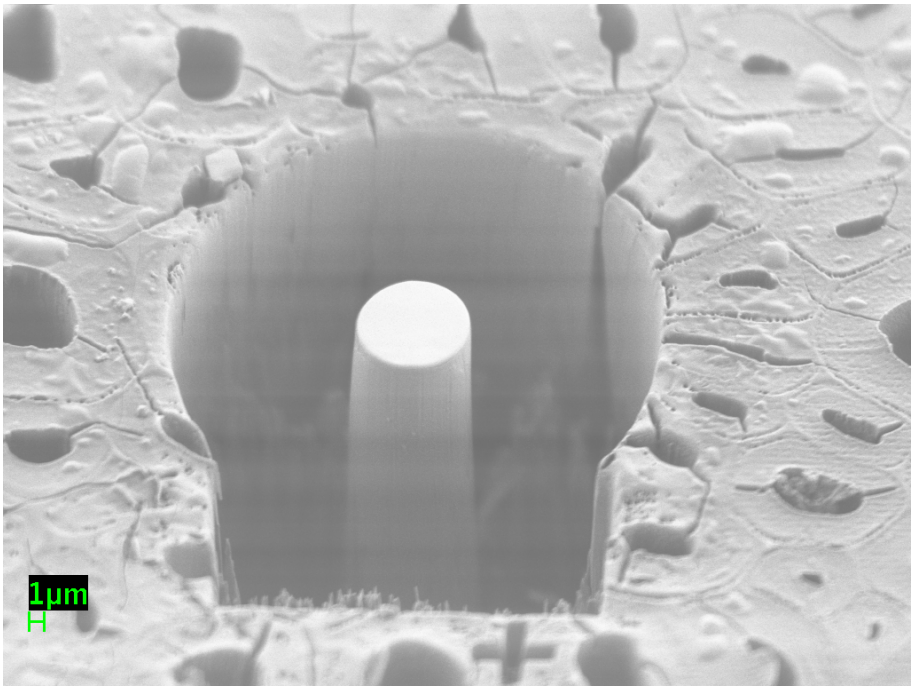

(a)

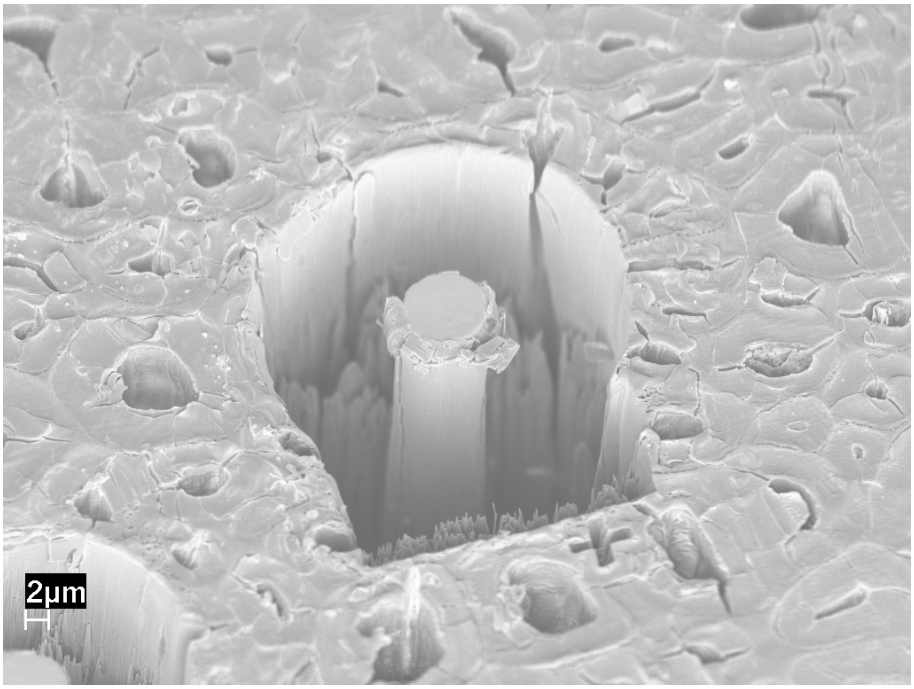

(b)

Figure 4-10. SEM image of the hardwood micropillar with 7.6 micrometers diameter at 36° tilt (a) before testing, (b) after testing

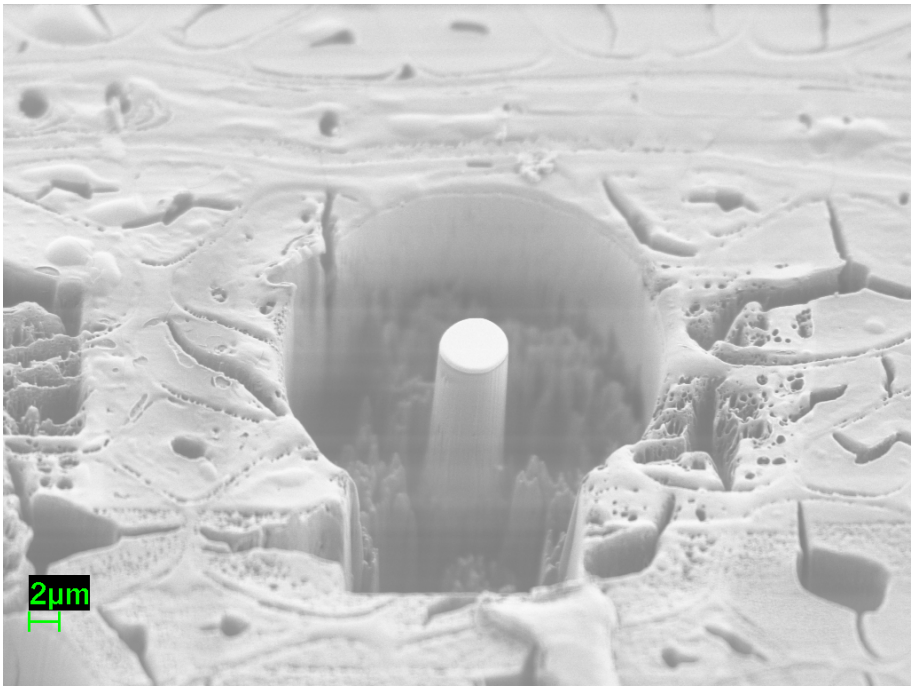

(a)

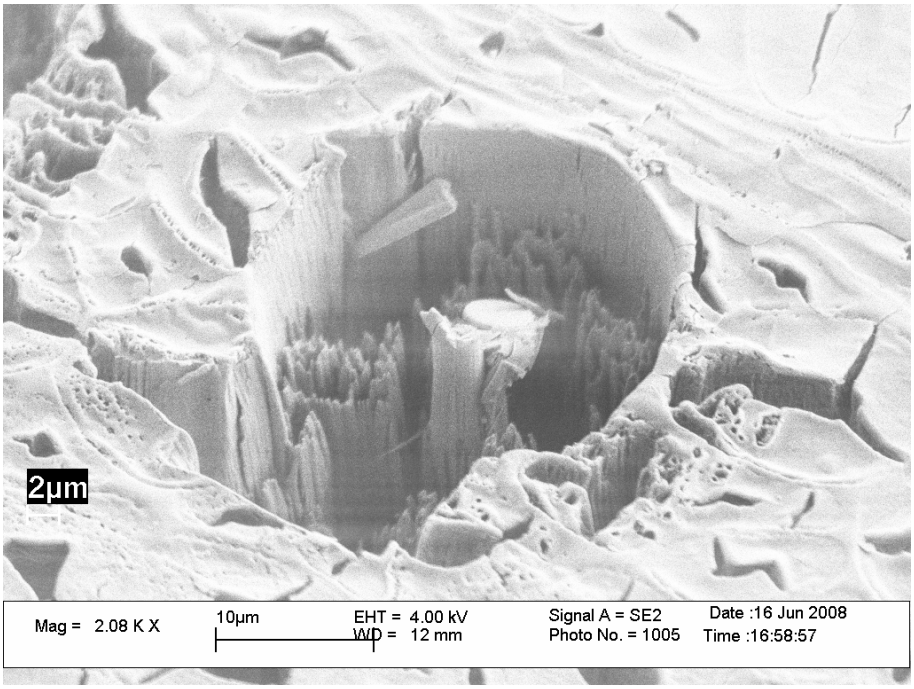

(b)

Figure 4-11. SEM image of the hardwood micropillar with 4.9 micrometers diameter at 36°tilt (a) before testing, (b) after testing

(a)

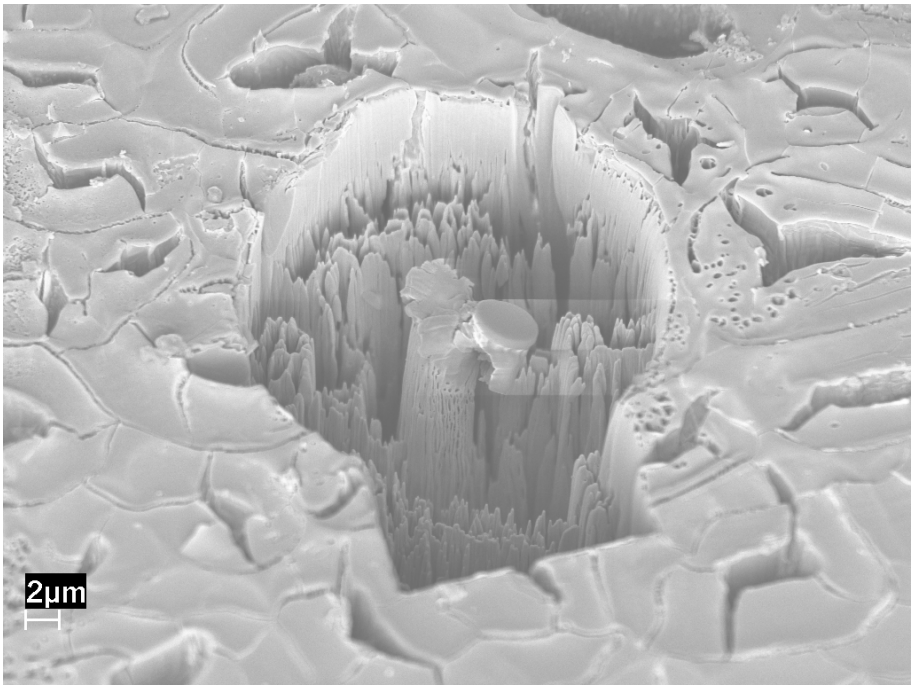

(b)

Figure 4-12. SEM image of the hardwood micropillar with 4.3 micrometers diameter at 36° tilt (a) before testing, (b) after testing

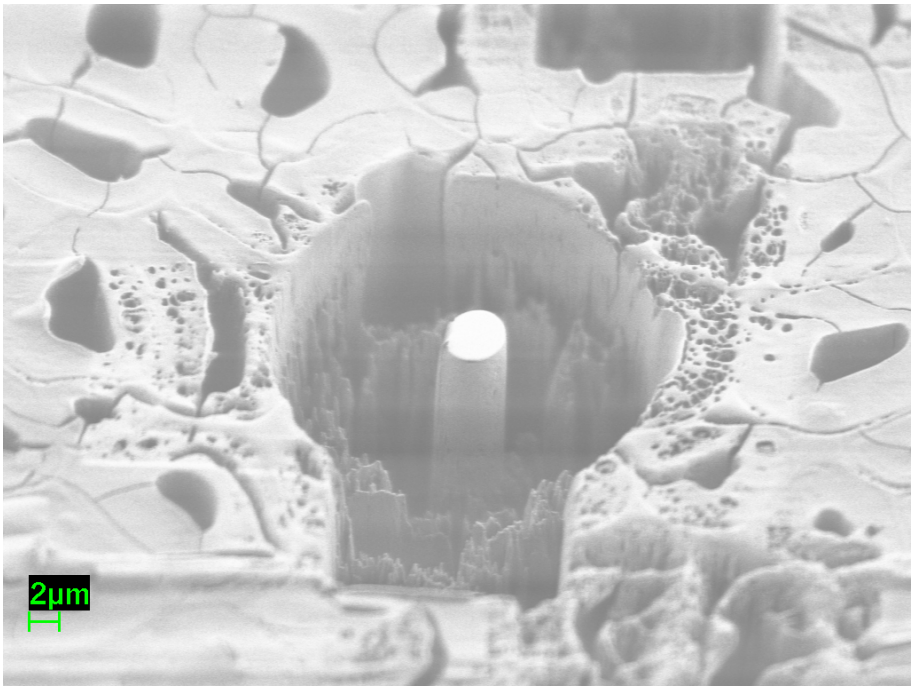

(a)

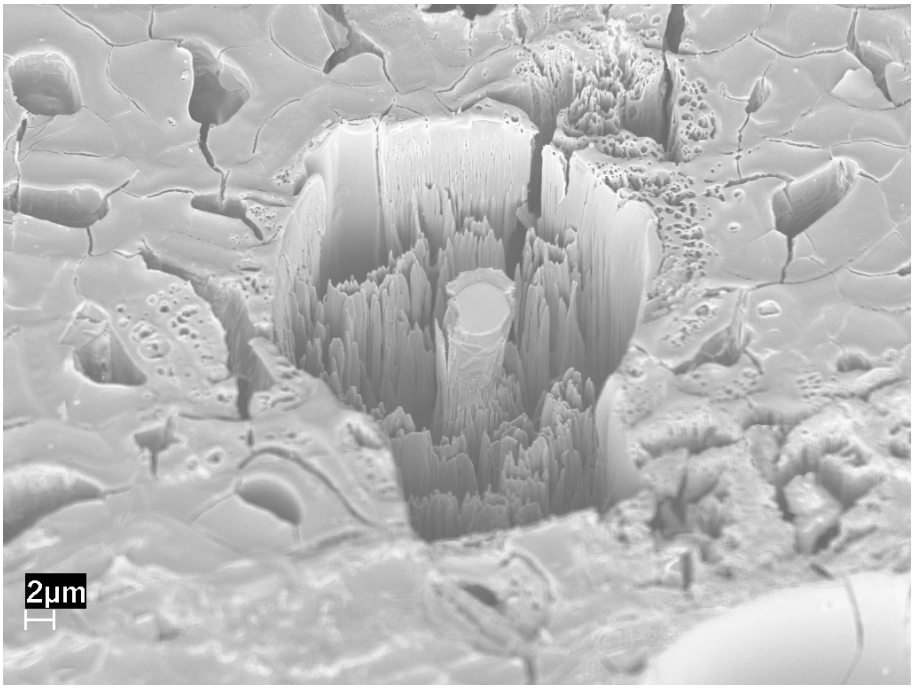

(b)

Figure 4-13. SEM image of the hardwood micropillar with 4.6 micrometers diameter at 36°tilt (a) before testing, (b) after testing

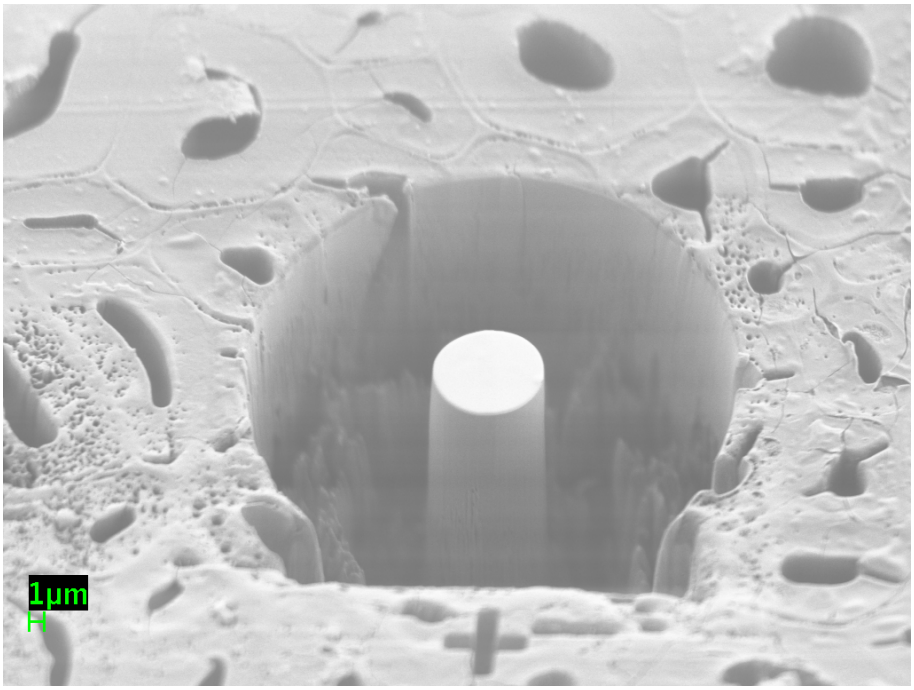

(a)

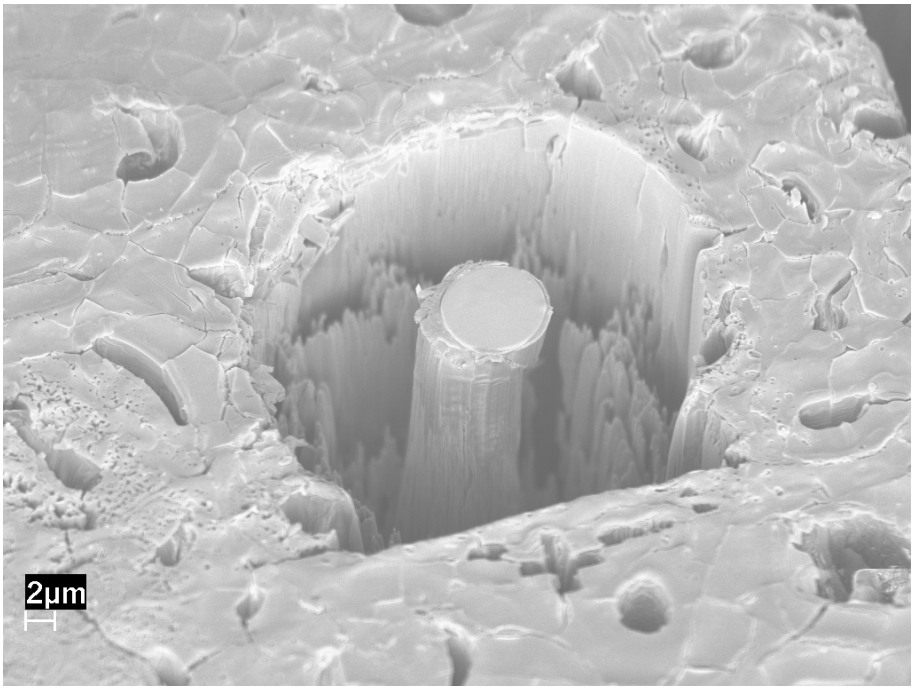

(b)

Figure 4-14. SEM image of the hardwood micropillar with 7.4 micrometers diameter at 36° tilt (a) before testing, (b) after testing

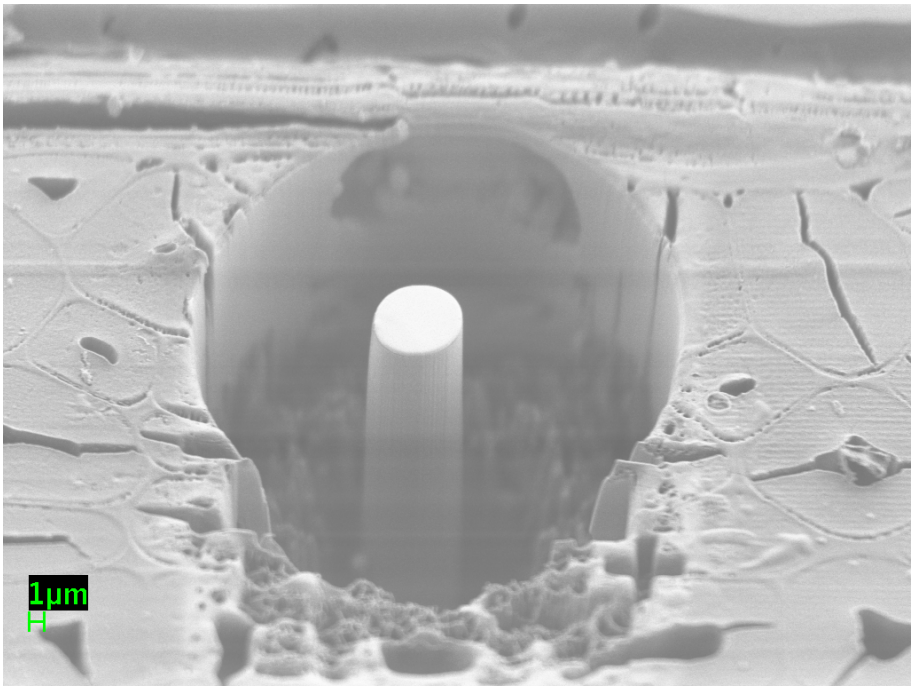

(a)

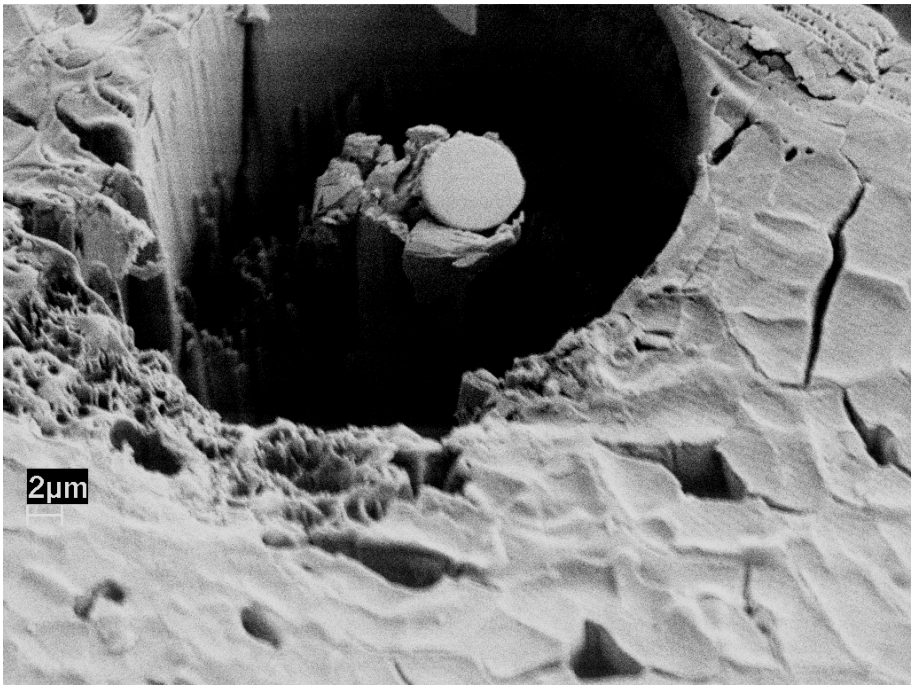

(b)

Figure 4-15. SEM image of the hardwood micropillar with 6.1 micrometers diameter at 36° tilt (a) before testing, (b) after testing

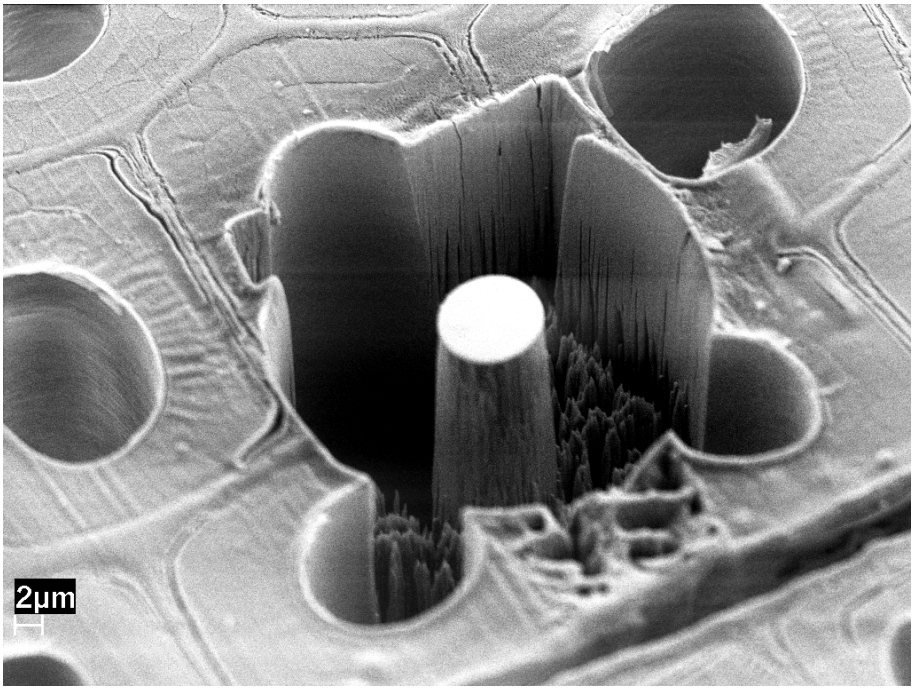

(a)

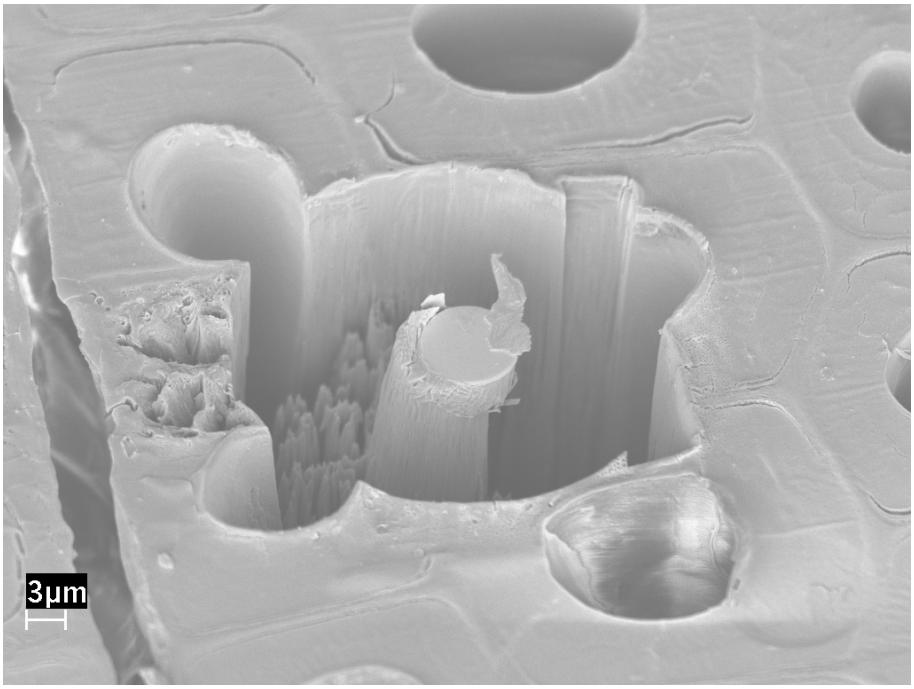

(b)

Figure 4-16. SEM image of the softwood micropillar with 7.4 micrometers diameter at 36° tilt (a) before testing, (b) after testing

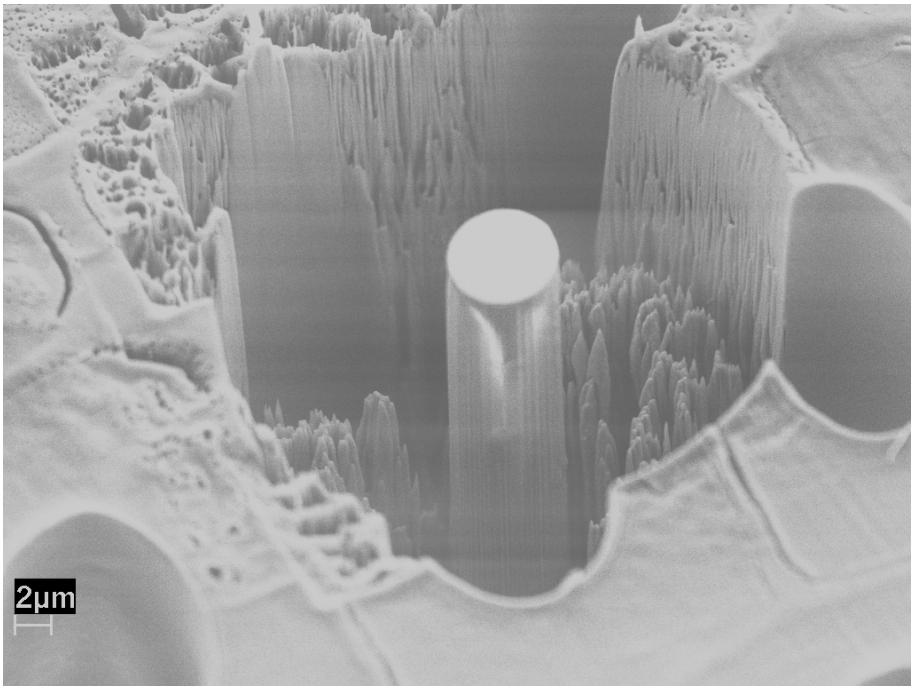

(a)

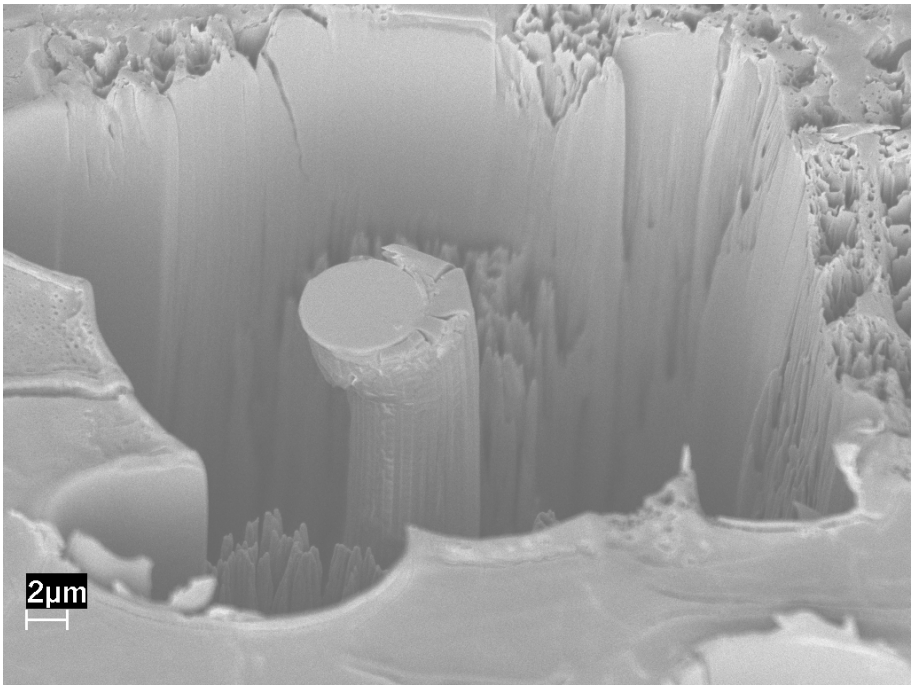

(b)

Figure 4-17. SEM image of the softwood micropillar with 5.9 micrometers diameter at 36° tilt (a) before testing, (b) after testing

From both images of hardwood and softwood, it was concluded that wood cell wall is a brittle material, which is the same as timber.

Some cracks in the cell wall near the micropillar in the hardwood specimen before compression test were noted, such as in Figure 4-8 and 4-9. This did not happen in the softwood specimen. This may be the result of a difference in the climate between Asia and North American. The weather in United States is generally dryer than in Asia. These cracks could also have been generated during the initial sample preparation process. When the latewood part was cut from the bulk sample, the excessive force could have caused inner-stress which generated these flaws.

4.3. Micropillar dimension measurement

As far as the pillar diameter measurement was concerned, according to several references, there were different ways to determine this diameter because of the imperfect shape of the micropillar. Uchic and Dimiduk (2005) took flat view SEM images at 0° tilt showed in Figure 4-18, the cross-sectional area of the micro-compression specimen was measured as pillar diameter. Moser et al. (2007) found that the diameter of micropillars varied along the axis (Figure 4-19). So the diameter has been measured, somewhat arbitrarily, near the lower end at about 20% of the height of the pillar. Volkert and Lilleodden (2006) took SEM images at 52° tilt (Figure 4-20). The column diameter, d, was defined as the diameter at half the column height.

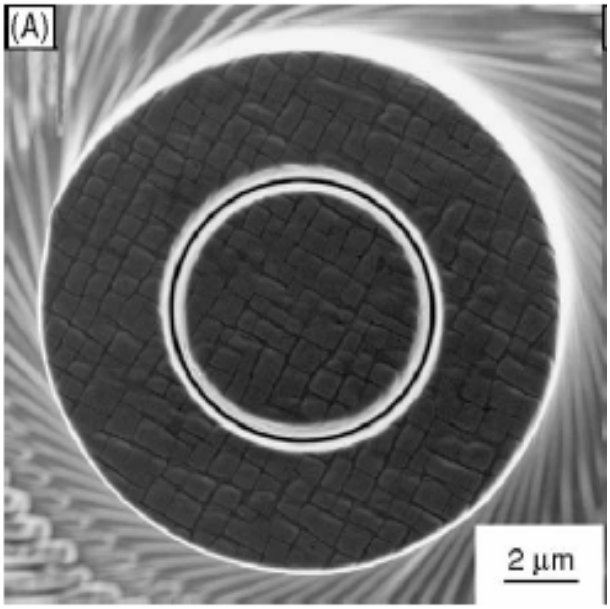

Figure 4-18. A Ni super alloy micro-sample that is approximately 9.6 micrometers in diameter (Uchic and Dimiduk 2005)

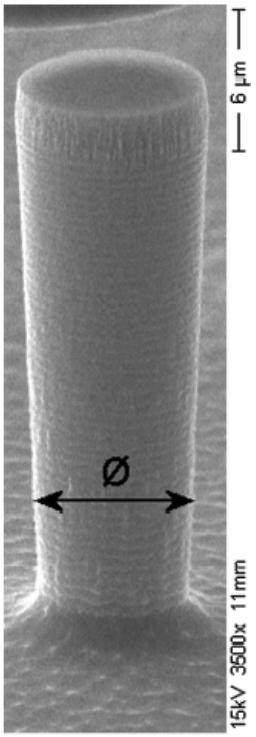

Figure 4-19. Si micropillar (Moser et al. 2007)

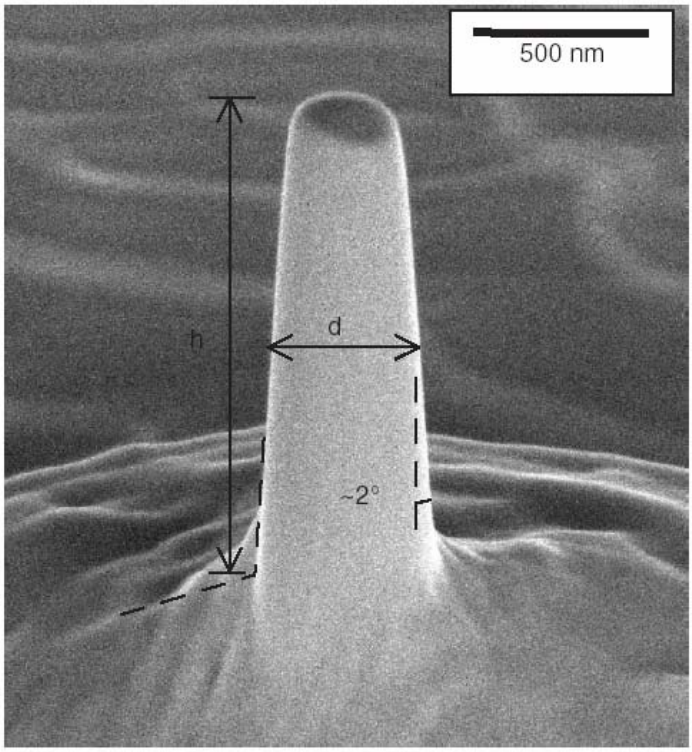

Figure 4-20. Single crystal Au columns (Volkert and Lilleodden 2006)

From the fracture behavior of hardwood and softwood micropillars, most cracks happened near the upper top at about 10% of the height of the pillar. So the diameter of micropillar was determined near fracture area, which could result in more accurate stress through calculation. The exact procedure was as follows: the sample was tilted at 36° and a SEM image of individual micropillar before test was taken. Then these images were analyzed by ImageJ (software), the length of the sidewall at 10% of the height of the pillar was measured as the diameter of micropillar.

The pillar length measurement needed a correction. First, the images of micropillars were taken at 36° tilt, the length x could be measured by ImageJ software.

The dimensions of the length, l, was then corrected for foreshortening using the relationship $l = x/\sin(36^{\circ})$.

4.4. Yield stress and compression strength

After SEM image checking, 11 hardwood micropillars and 5 softwood micropillars were compressed correctly and the corresponding data was selected and analyzed. Figure 4-21 shows the load-displacement curves of four successful micropillar compression tests in which (a) and (b) are from keranji micropillars, (c) and (d) are from loblolly pine micropillars. Each curve could be generally characterized as (1) elastic loading, (2) followed by a transition to onset of plastic deformation, (3) stable flow load and holding, (4) unloading. The compressive loads of every micropillar were different because of the different micropillar diameters. Normally the larger micropillar diameter will result in larger compressive load.

During the compression test, when the maximum load reached, the micropillar was destroyed and lost resistance simultaneously, the displacement increased a lot in the short time and only a few data was recorded during this period. The compression depths of each micropillar were different due to the different pillar length. As a result, the compression conditions were different. Compression test in the figure 4-21 (a) stopped right after the pillar was broken, the corresponding SEM image of broken micropillar is showed in Figured 4-8. The micropillar in the figure 4-21 (b) was over-compressed as the displacement was larger than 10 micrometers, which was much larger than the desired compression depth. The corresponding SEM image is in Figure 4-15.

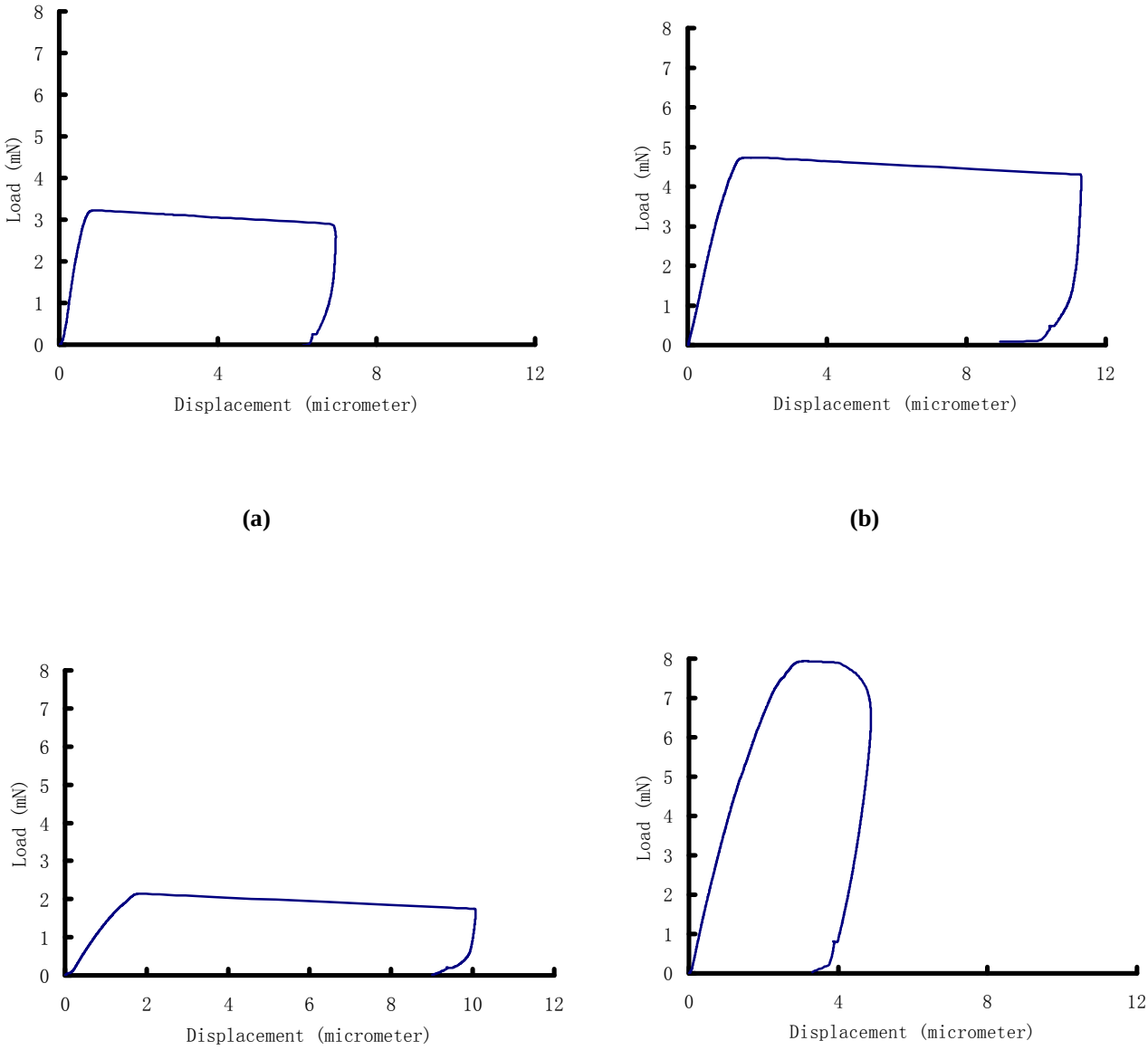

Figure 4-21. Compressive load-displacement curve of keranji and loblolly pine

(a) keranji micropillar with 4.75 micrometers diameter;
(b) keranji micropillar with 6.1 micrometers diameter;
(c) loblolly pine micropillar with 5.3 micrometers diameter;
(d) loblolly pine micropillar with 7.4 micrometers diameter

The loblolly pine micropillars had similar compression conditions. The micropillar in compression test figure 4-21 (c) was over-compressed. The compression test in figure 4-21 (d) stopped right after the micropillar was destroyed and the corresponding SEM image is in Figure 4-16. The yield stress and compression strength could be analyzed in the stress-strain graph which was converted from the load-displacement curve.

Yield stress is a very important parameter of the material for engineering design. Yield stress ideally is the point between the elastic deformation and plastic deformation. Here the yield point was defined as the point at the end of the linear-elastic relationship between the stress and strain, and the point at the initiation where the slope of the stress and strain curve steadily decreased with increasing stress (Yoshihara and Ohta 1997). In the reality, there are several methods to determine yield stress as showed in Figure 4-22.

In the "non-offset" method, yield stress is chosen as the branching point of the elastic line and the stress-strain curve, which is the Point P_0 in Figure 4-22. Reily and Burstein defined the yield stress as the point at the intersection point between the two straight line segments through the pre- and post- yield elastic portions of the stress-strain curve, which is P_{RB}.

Another one is "strain offset" method. The yield stress here is determined from the intersection point of the stress-strain curve and a straight line offset in the several value of strain, which is P_{OFF}. Normally the offset volume is 0.2-0.3%.

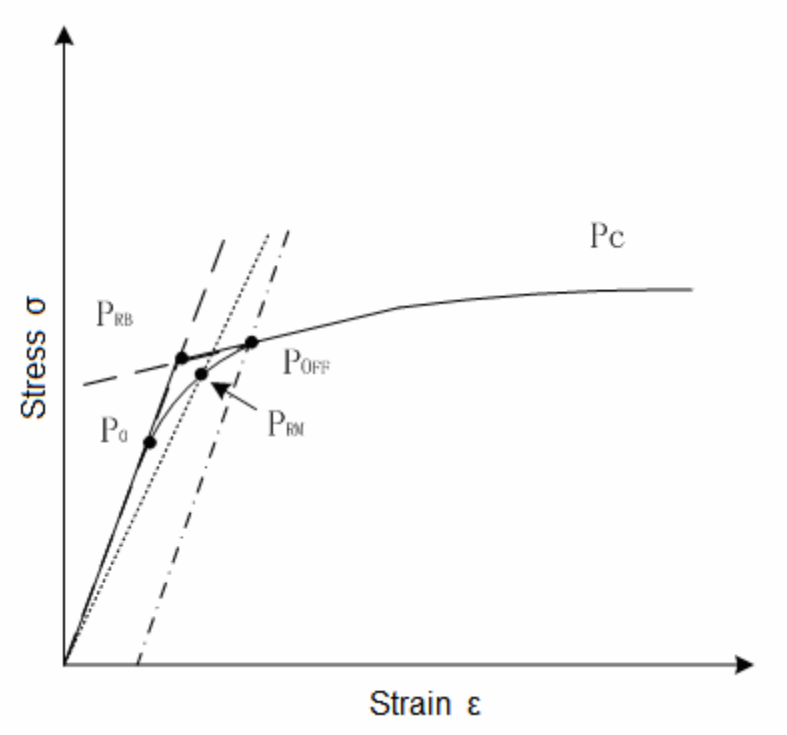

Figure 4-22. Stress and Strain curve

The "reduced modulus method" is from Japan Industrial Standard Z 2111. The yield stress is defined as the intersecting point of the stress-strain curve and a straight line drawn by reducing the elastic modulus a certain percentage, $P_{RM.}$ The reduced value is about 3-5% generally.

In this research the "offset method" was chosen to determine the yield stress, which was the most common method used by other researchers. The offset volume was 0.2%. Figure 4-23 shows the yield stress of both hardwood and softwood samples. 11 hardwood micropillars and 5 softwood micropillars were compressed correctly from all the qualified micropillars. From this graph, it was found that there was no obvious relationship between the yield stress and pillar diameter. The yield stress of hardwood

ranged from 118.3 MPa to 152.7 MPa for micropillar diameters of 4.63 micrometers to 7.63 micrometers. The yield stress of hardwood ranged from 94.3 MPa to 130.7 MPa for micropillar diameter of 5.21 micrometers to 8.19 micrometers.

Compression strength is the maximum stress a material can sustain under crush loading. In Figure 4-22, compression strength is the stable flow stress after the plastic deformation, which is Point P_c. Compressive strength also can be calculated by dividing the maximum load by the original cross-sectional area of the specimen in a compression test.

Figure 4-24 shows the compression strength of the keranji and loblolly pine. The compression strength of hardwood ranged from 127.9 MPa to 185.6 MPa for micropillar diameter of 4.63 micrometers to 7.63 micrometers. The compression strength of the hardwood ranged from 96.4 MPa to 155.7 MPa for micropillar diameter of 5.21 micrometers to 8.19 micrometers.

The variation in compression strength within a species was large. For example, even in the micropillars with similar diameter (between 4.62 and 4.87 micrometers), the difference in compression strength was about 57 MPa. This may due to the inhomogeneous characters of the wood cell wall. Because wood cell is a natural composite, the composition of cellulose, hemicellulose and lignin is different even in the same cell wall (Bowyer et al. 2003).

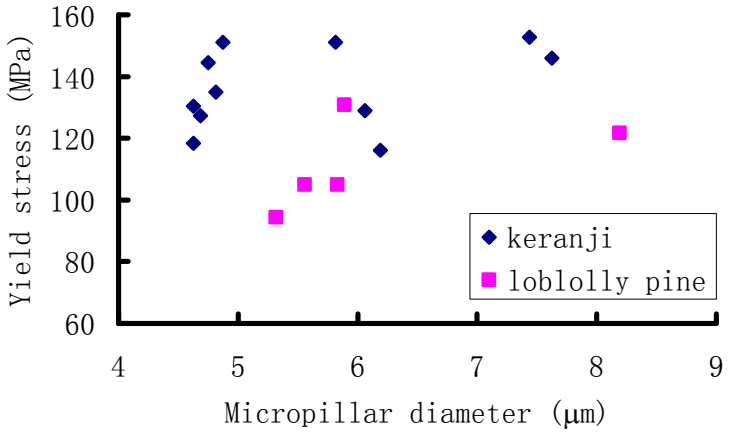

Figure 4-23. Yield stress of hardwood and softwood micropillar

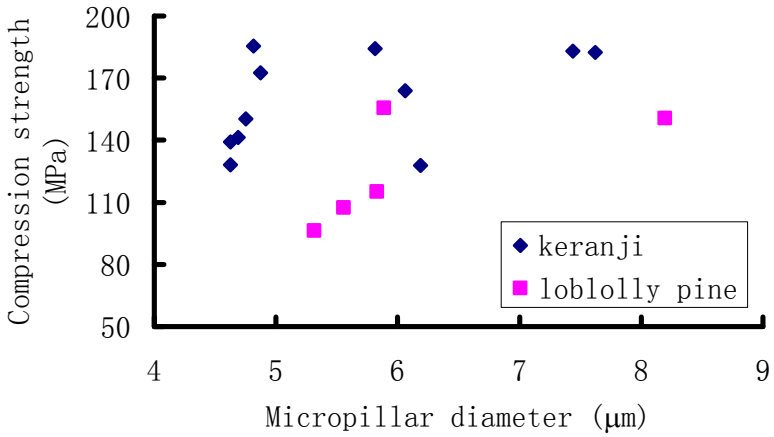

Figure 4-24. Compression strength hardwood and softwood micropillar

To predict the compression strength of wood cell wall and investigate the reliability of the data from the micropillar compression test, a model which showed the relationship between compression strength and specific density was established in Figure 4-22. The compression strength and specific gravity of 111 representative wood species of both hardwood and softwood in North America were collected. The data sources came from Wood handbook (1999), the encyclopedia of wood (1989) and ASTM D2555 (Standard Practice for Establishing Clear Wood Strength Values).

From this model, it was found that normally the compression strength increases with increasing specific density. A linear trendline was added to the data. The equation of this line was y=64.947x+11.134 (R^2 = 0.7042).

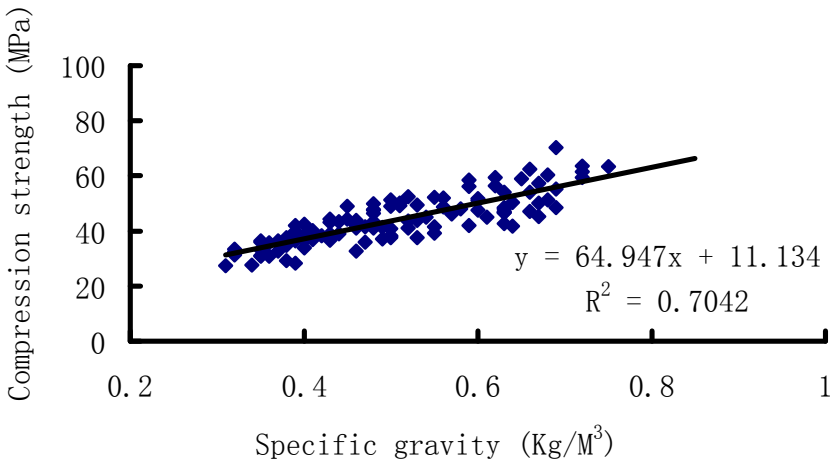

Figure 4-25. Compression strength vs. specific density model

In this equation, x is the specific density and y is the corresponding compression strength. It is well known that, the density of wood cell wall is 1.5 kg/m^3 in theory. If x is assumed equal to 1.5, then compression strength, y, is 108.5 MPa.

The compression of timber is different from the compression of wood cell wall. Timber is a porous material. When the compressive load was added to bulk sample from timber, weaker part, like the lignin between the nearby cell walls, for example, could be destroyed first. Wood cell wall is a solid material, through the micropillar compression test, the damage could only happen in cell wall material. So the compression strength of wood cell wall should be a little bit higher than the one from this model even they have the same density.

The results (Table 4-1) showed that the average yield stress of loblolly pine was 111.3 MPa with the standard deviation 14.6 MPa, and the average yield stress of keranji was 136.5 MPa while the standard deviation was 13.2 MPa. The average compression strength of loblolly pine is 125.0 MPa with the standard deviation 26.5 MPa. The average compression strength of keranji was 160.0 MPa while the standard deviation was 23.1 MPa.

Table 4-1. Mechanical properties of wood cell wall (data in the parentheses is Standard Deviation)

Species	Yield stress (MPa)	Compression strength(MPa)	Number of valid test
loblolly pine	111.3 (14.63)	125 (26.58)	5
keranji	136.5 (13.26)	160 (23.16)	11

In Figure 4-25, the compression strength of clear loblolly pine at 12% moisture content (MC) is 49.2 MPa which is obviously much lower than the one of loblolly pine cell wall. The compression strength of both hardwood and softwood were higher than one predicted by the model, which is about 108.5 MPa. It can be concluded that the data from this experiment were reliable.

It was found that both the yield stress and the compression strength for keranji cell wall were higher than for loblolly pine cell wall. This could be explained as following. First, the density of keranji timber is 1.05 kg/m^3 while the one of loblolly pine is 0.51 kg/m^3 (Wood hand book, 1999). According to the model showed in Figure 4-25, the strength of keranji timber should be larger than the one of loblolly pine. The cell wall of keranji should be densier than one of loblolly pine. Secondly, the MFA has been considered as an important factor that determines wood properties. It was also found that, the MFA increases (to a value up to 90º), the longitudinal stiffness would decrease significantly (Tze et al. 2007). If this phenomenon can also be applied to other mechanical properties, it will also confirm this conclusion, because the MFA of this keranji cell wall is 5.9° (Wu et al. 2008) and the correspongding MFA of loblolly pine cell wall is 15°(Tze et al. 2007). Obviously the MFA of loblolly pine cell wall is much larger than the MFA of keranji cell wall. Third, from nanoindentation test, the modulus of keranji cell wall was larger than the modulus of loblolly pine cell wall. All these confirm that the mechanical properties of keranji cell wall are higher than the ones of loblolly pine cell wall.

4.5. Engineering modulus

The engineering modulus was measured through a continuous micropillar compression test. Figure 4-26 shows the load-displacement curve of both samples while the compression depth of each cycle was 200 nm, 400 nm and 600 nm respectively. In the continuous compression test, the elastic region could be confirmed more clearly by comparing the 3 compression cycling. Through this figure, the cycle 1 curve was sure to be elastic region, so the loading part in cycle 1 curve was used to calculate the engineering modulus.

Figure 4-27 shows the engineering modulus of both keranji and loblolly pine from micro compression test with the modulus of the same species from nanoindentation test. The engineering modulus of keranji was 7.7 GPa and the one of loblolly pine was 4.5 GPa. The modulus of keranji from nanoindentation test was 24.6 GPa and the one of loblolly pine was 17.6 GPa. The engineering modulus should be similar to the nanoindentation based modulus because they are the same mechanical properties acquired via different measurement method. But here the modulus data was much higher than engineering modulus.

It was found that the data of engineering modulus was not as accurate as modulus because of the limitation of experiment condition. The engineering modulus was defined as the stress divided by strain in the elastic region. Because the stress data were reliable, the problem may be due to the strain. The strain is the deformation divided by the original pillar length. The pillar length data were not accurate as expected.

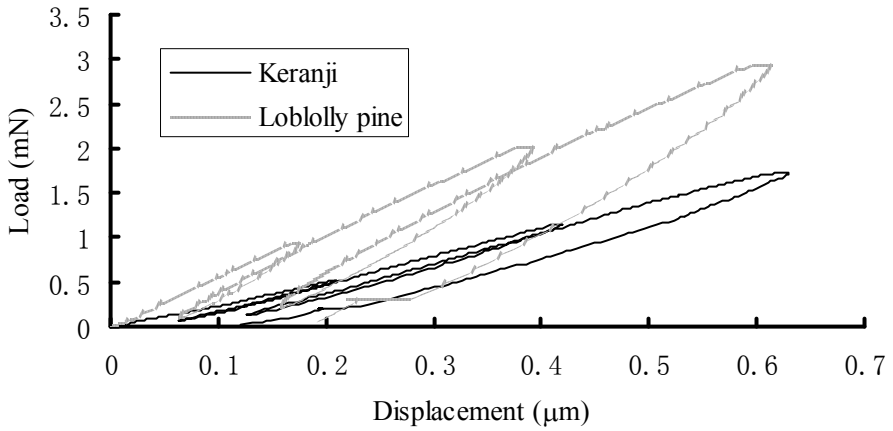

Figure 4-26. Continuous compressive load-displacement curve of keranji and loblolly pine

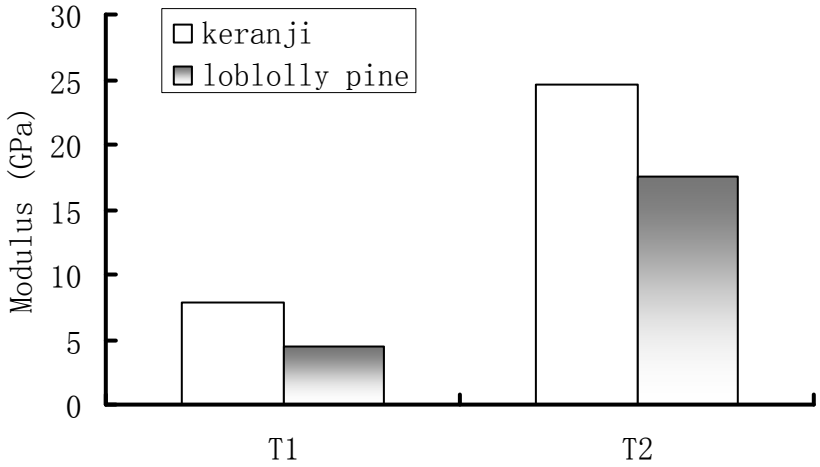

Figure 4-27. Comparison of modulus between keranji and loblolly pine
(T1-micro compression test, T2-nanoindentation test)

In the timber compression test, the dimension of sample specimen could be measured easily and directly. A strain gage could also be attached to the specimen which could record the exact strain change during the test (Figure 4-28). In the micro-compression test, as mentioned before, the dimension of micropillar could only be measured by analyzing SEM image via ImageJ software. The accelerating voltage of FIB system used for sample preparation here was fixed at 30 KV. This voltage could mill samples relatively quickly, but the bottom of the micropillars were not very clear which made it difficult to accurately determine the pillar length .

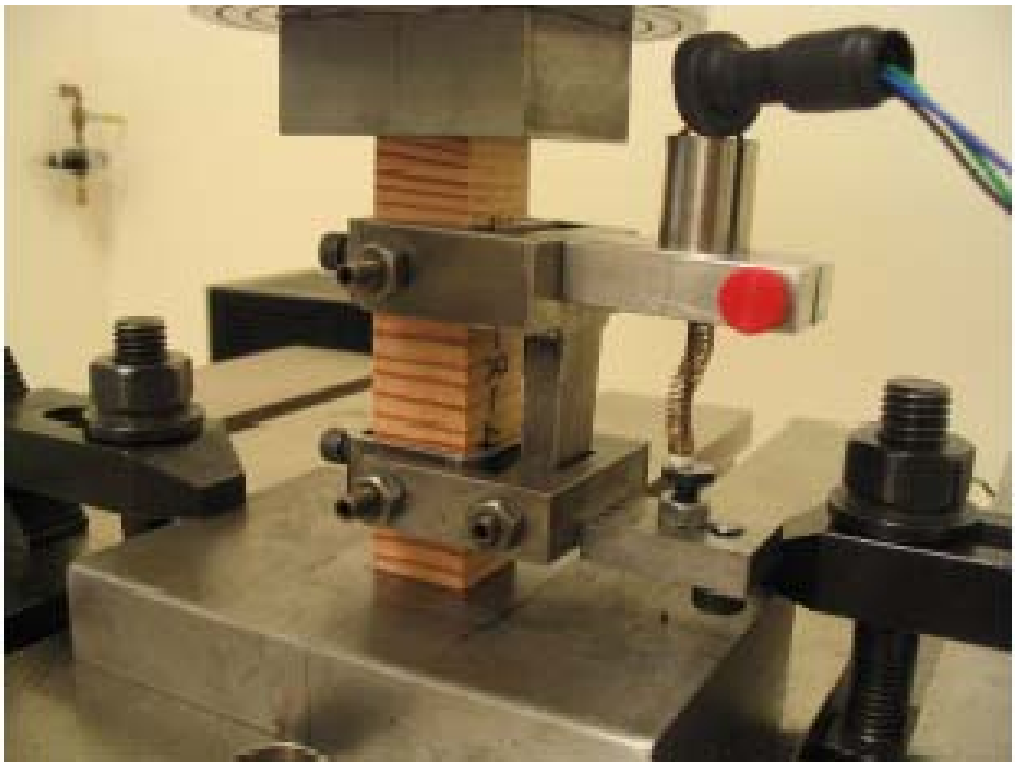

Figure 4-28. Macro scale wood compression test (Hong and Barrett, 2006)

CHAPTER 5 CONCLUSIONS AND RECOMMENDATIONS

5.1. Conclusions

This project investigated important properties of wood cell wall which was measured for first time using a uniaxial micro-compression test. FIB system is found to be a useful instrument suitable for wood material sample preparation. The cylindrical shaped micro pillars were milled successfully by FIB while each pillar was milled in a single wood cell wall. SEM images of each micropillar were analyzed by ImageJ software, the dimension of the micropillar was measured through this method.

Uniaxial compression test was performed on each qualified micropillar and all these micropillars after test were evaluated again by SEM images to make sure the compression test was performed correctly. The fracture behavior of wood micropillar confirmed that wood cell wall is also a brittle type of material.

The data corresponding to the correctly compressed micropillars were collected and analyzed. The yield stress of keranji wood cell wall was 136.5 MPa and the compression strength was 160 MPa. The yield stress of loblolly pine wood cell wall was 111.3 MPa and the compression strength was 125 MPa. The engineering modulus from the compression test was not accurate due to the limitation of the experimental conditions.

5.2. Recommendations

This research successfully investigated some important properties of wood cell wall through uniaxial compression test for first time. But due to the limited time to use FIB for sample preparation, only one species of hardwood and one species of softwood were chosen to do the test in this project.

In the future work, more wood species should be chosen to perform the micro-compression test to collect more data. The hardwood specimen and softwood specimen from same growth ring will be prepared for the test. It is interesting to study whether there are any difference between the mechanical properties of hardwood cell wall and softwood cell wall with same MFA.

The dimension of pillars prepared in this research was in micro-scale. The pillar dimension will be reduced to nano-scale in future. The mechanical properties of nano-pillar will be investigated and also be compared with the one of micropillar to investigate whether the "size effect" happens in cell wall material.

The engineering modulus of wood cell wall was not accurate in this project. The precision of this data may be improved by using more advanced equipment in future. Now in the advanced FIB system, the accelerating voltage is flexible which is from 5 KV to 30 KV. During the sample preparation, the high voltage (30 KV) could be used first to mill the shape of micropillar, then a low voltage (5 KV, for example) should be used to smooth the bottom of micropillar. In this way, a clear foundation may be generated and

the length of the micropillar could be measured more accurately. *In-situ* experiment is more popular now. There is a SEM video system built in advanced indentation system, which can record the whole process of micro compression test. SEM images with a scale of the same micro pillar could be acquired from the video, so the deformation of the pillar during the compression test could be calculated accurately.

LITERATURE CITED

ASTM. 2001. Standard practice for establishing clear wood strength values1. ASTM D2555-06. American Society for Testing and Materials, Philadelphia, PA, USA.

Bariska, M., and L. J. Kucera, Zurich. 1985. On the fracture morphology in wood Part 2: Macroscopical deformations upon ultimate axial compression in wood. Wood Science and Technology 19:19-34.

Bei, H., S. Shim, E. P. George, M. K. Miller, E. G. Herbert, G. M. Pharr. 2007. Compressive strength of molybdenum alloy micropillars prepared using a new technique. Scripta materials 57:397-400.

Bei, H., and S. Shim. 2007. Effects of focused ion beam milling on the nanomechanical behavior of a molybdenum-alloy single crystal. Applied physics 91:111915

Boey, F. Y. C., L. H. L. Chia, S. H. Teoh. 1985. Compression, bend, and impact testing of some tropical wood-polymer composites. Radiat of physics and chemistry 4: 415-421.

Bowyer, J. L., R. Shmulsky, J. G. Haygreen. 2003. Forest products and wood science-an introduction. Fourth edition.

Cheng, Q. and S. Wang. 2008. A method for testing the elastic modulus of single cellulosic fibrils via atomic force microscopy. Composites Part A: Applied Science and Manufacturing (in print).

Cockrell, R. A., and R. M. Knudson. 1973. A comparison of static bending, compression and tension parallel to grain and toughness properties of compression wood and normal wood of a giant sequoia. Wood science and technology 7: 241-250.

Drobne, D., M. Milani, A. Zrimec, V. Leser, M. B. Zrimec. 2005. Electron and ion imaging of gland cells using the FIB/SEM system. Journal of microscopy 219:29-35.

Eberhardt, T. L. 2007. A reassessment of the compression strength properties of southern yellow pine bark. Forest Products Journal 57(4):95-97.

Field, R. D., and P. A. Papin. 2004. Location specific in situ TEM straining specimens made using FIB. Ultramicroscopy 102: 23-26.

Gasser, P., U. E. Klotz, F. A. Khalid, O. Beffort. 2004. Site-specific Specimen Preparation by Focused Ion Beam Milling for Transmission Electron Microscopy of Metal Matrix Composites. Microscopy and Microanalysis 10:311-316.

Giannuzzi, L. A., and F. A. Stevie. 1999. A review of focused ion beam milling techniques for TEM specimen preparation. Micron 30:197-204.

Giannuzzi, L. A., L. J. Drown, S. Brown, R. Irwin, F. A. Stevie. 1998. Application of the FIB lift-out technique for TEM specimen preparation. Microscopy Research and Technique 41:285-290.

Gindl, W., and H. S. Gupta. 2002. Cell-wall hardness and Young's modulus of melamine-modified spruce wood by nano-indentation. Composites: Part A 33:1141-1145.

Gindl, W., H. S. Gupta, T. Schoberrl, H. C. Lichtenegger, P. Fratzl. 2004. Mechanical properties of spruce wood cell walls by nanoindentation. Applied Physics A 79: 2069-2073.

Gomez, S., and D. Svecova. 2008. Behavior of split timber stringers reinforced with external GFRP sheets. Journal of Composites for Construction 3: 202-211.

Gong, A., D. P. Kamdem, R. Harichandran, 2004. Compressive tests on wood-cement particle composites made of CCA-treated wood removed from service. Environmental Impacts of Preservative-Treated Wood Conference, Orlando, FL.

Greer, J. R., W. C. Oliver, W. D. Nix. 2005. Size dependence of mechanical properties of gold at the micron scale in the absence of strain gradients. Acta materialia 53:1821-1830.

Hata, S., H. Sosiati, N. Kuwano, M. Itakura, T. Nakano, Y. Umakoshi. 2006. Removing focused ion-beam damages on transmission electron microscopy specimens by using a plasma cleaner. Journal of electron microscopy 55:123-26.

Heaney, P. J., E. P. Vicenzi, L. A. Giannuzzi, K. J. T. Livi. 2001. Focused ion beam milling: A method of site-specific sample extraction for microanalysis of Earth and planetary materials. American Mineralogist 86:1094–1099.

Hoffmeyer, P., L. Denmark, R. W. Davidson, N. Y. Syracuse. 1989. Mechano-sorptive creep mechanism of wood in compression and bending. Wood Science and Technology 23:215-227.

Hong, J. P., and J. D. Barrett. 2006. Empirical wood material model for three dimensional finite element analysis of a nail joint. WCTE 2006-Proceedings of 9th World Conference on Timber Engineering, Portland, USA.

Hwang, G. S., J. C. Hsiung, M. Y. Kuo. 2001. Changes in surface temperature of wood specimens during compression testing. Taiwan Forestry Science 16:125-132.

Ishitani, T., H. Hirose, H. Tsuboi. 1995. Focused-ion-beam digging of biological specimens. Journal of Electron Microscope 44:110-114.

Jakes, J. E., D. S. Stone, C. R. Frihart. 2007. Nanoindentation size effects in wood. 30th annual meeting of the adhesion society, Tampa Bay, FL. P15-17.

Kaegi, R., and P. H. Gasser. 2006. Application of the focused ion beam technique in aerosol science: detailed investigation of selected, airborne particles. Journal of Microscopy 224:140-145.

Kamino, T., T. Yaguchi, T. Ohnishi, T. Ishitani, M. Osumi. 2004. Applications of a FIB-STEM system for 3D observation of a resin-embedded yeast cell. Journal of Electron Microscopy 53:563-566.

Keckes, J., I. Burgret, K. Fruhmann, M. Muller, K. Kolln, M. Hamilton, M. Burghammer, S. Roth, S. S. Tschegg, P. Fratzl. 2003. Cell-wall recovery after irreversible deformation of wood. Nature Materials 2: 810-814.

Ko, D. S., Y. M. Park, S. D. Kim, Y. W. Kim. 2007. Effective removal of Ga residue from focused ion beam using a plasma cleaner. Ultramicroscopy 107:368-373.

Koch, P. 1985. Utilization of hardwoods growing on southern pine sites. U.S. Dep. Agric. For. Serv., Handb. 605 3710 p.3 vol. U.S. Govt. Print. Off., Washington, D.C.

Konnerth, J., and W. Gindl. 2006. Mechanical characterization of wood-adhesive interphase cell walls by nanoindentation. Holzforschung 60: 429-433

Konnerth, J., A. Valla, W. Gindl. 2007. Nanoindentation mapping of a wood-adhesive bond. Applied Physics A 88: 371-375.

Korkut, S., and B. Guller. 2008. Physical and mechanical properties of European Hophornbeam (Ostrya carpinifolia Scop.) wood. Bioresource Technology 99: 4780-4785.

Kucera, L. J., and M. Bariska. 1982. On the fracture morphology in wood Part 1: A SEM-study of deformations in wood of spruce and aspen upon ultimate axial compression load. Wood Science and Technology 16:241-259.

Lanford, R. M., and C. Clinton. 2004. In situ lift-out using a FIB-SEM system. Microns 35:607-611.

Lee, S. H., S. Wang, G. M. Pharr, M. Kant, D. Penumadu. 2007a. Mechanical properties and creep behavior of lyocell fibers by nanoindentation and nano-tensile testing. Holzforschung 61:254-260.

Lee, S. H., S. Wang, G. M. Pharr, H. Xu. 2007b. Evaluation of interphase properties in a cellulose fiber-reinforced polypropylene composite by nanoindentation and finite element analysis. Composites Part A: Applied Science and Manufacturing 38:1517-1524.

Lourenco, P. B., A. O. Feio, J. S. Machado. 2007. Chestnut wood in compression perpendicular to the grain: Non-destructive correlations for test results in new and old wood. Construction and Building Materials 21:1617–1627.

Marko, M., C. Hsieh, R. Schalek, J. Frank, C. Mannella. 2007. Focused–ion-beam thinning of frozen-hydrated biological specimens for cryo-electron microscopy. Nature Methods 4:215-217.

Matsui, S., and Y. Ochiai. 1996. Focused ion beam applications to solid state devices. Nanotechnology 7:247-258.

Michler, J., K. Wasmer, S. Meier, F. Ostlund. K. Leifer. 2007. Plastic deformation of gallium arsenide micropillars under uniaxial compression at room temperature. Applied Physics Letters 90: 043123.

Moghadam, S. H., R. Dinarvand, L. H. Cartilier. 2006. The focused ion beam technique: A useful tool for pharmaceutical characterization. International Journal of Pharmaceutics 321:50-55.

Moser, B., K. Wasmer, L. Barbieri, J. Michler. 2007. Strength and fracture of Si micropillars: a new scanning electron microscopy-based micro-compression test. Journal of Material Research 22(4): 1004-1011.

Navaranjan, N., R. J. Blaikie, A. N. Parbhu, J. D. Richardson, A. R. Dickson. 2008. Atomic force microscopy for the measurement of flexibility of single softwood pulp fibres. Journal of Material Science 43: 4323-4329.

Oliver, W. C., and G. M. Pharr. 1992. An improved technique for determining hardness and elastic modulus using load and displacement sensing indentation experiments. Journal of Materials Research 7(6): 1564-1583.

Orso, S., U. G. K. Wegst, E. Arzt. 2006. The elastic modulus of spruce wood cell wall material measured by an in situ bending technique. Journal of Material Science 41:5122-5126.

Phaneuf, M. W. 1999. Applications of focused ion beam microscopy to materials science specimens. Micron 30:277-288.

Reyntjens, S., and R. Puers. 2001. A review of focused ion beam applications in microsystem technology. Journal of Micromechanics and Microengineering 11:287-300.

Rubanov, S., and P. R. Munroe. 2004. The application of FIB milling for specimen preparation from crystalline germanium. Micron 35: 549-556.

Seeling, U. 1998. Bending characteristics of Hickory (Carya ovata K. Koch) wood grown in Germany. Wood Science and Technology 32: 367-372.

Shipsha, A., and L. A. Berglund. 2007. Shear coupling effects on stress and strain distributions in wood subjected to transverse compression. Composites Science and Technology 67:1362-1369.

Shupe, T. F., L. H. Groom, T. L. Eberhardt, T. C. Pesacreta, T. G. Rials. 1997. Selected mehcnical and physical properties of Chinese tallow tree juvenile wood. Forest Products Journal 58(4): 90-93.

Spur, A. R. 1969. A low-viscosity epoxy resin embedding medium for electron microscope. Journal of Ultrastructure Research 26:31-43.

Stevie, F. A., C. B. Vartuli, L. A. Giannuzzi, T. L. Shofner, S. R. Brown, B. Rossie, F. Hillion, R. H. Mills, M. Antonell, R. B. Irwin, B. M. Purcell. 2001. Application of focused ion beam lift-out specimen preparation to TEM, SEM, STEM, AES and SIMS analysis. Surface and Interface Analysis 31:345-351.

Stokke, D. D., and L. H. Groom. 2006. Characterization of the cellulosic cell wall. Blackwell Publishing Professional, Iowa, USA.

Sugiyama, M., and G. Sigesato. 2004. A review of focused ion beam technology and its applications in transmission electron microscopy. Journal of Electron Microscopy 53(5): 527-536.

Swadener, J. G., E. P. George, G. M. Pharr. 2002. The correlation of the indentation size effect measured with indenters of various shapes. Journal of the Mechanics and Physics of Solids 50:681 – 694.

Tze, W. T. Y., S. Wang, T. G. Rials, G. M. Pharr, S. S. Kelley. 2007. Nanoindentation of wood cell walls: Continuous stiffness and hardness measurements. Composites: Part A 38:945-953.

Uchic, M. D., and D. M. Dimiduk. 2005. A method to investigate size effects in crystalline plasticity using uniaxial compression testing. Material Science and Engineering A 400-401: 268-278.

Volkert, C. A., and E. T. Lilleodden. 2006. Size effects in the deformation of sub-micron Au columns. Philosophical magazine 86:567-5579.

Walker, J. F., and R. F. Broom. 1997. Surface damage of semiconductor TEM samples prepared by focused ion beams. Institute of Physics Conference Series 157: 473-478.

Wimmer, R., B. N. Lucas, T. Y. Tsui, W. C. Oliver. 1997. Wood Science and Technology 31:131-141.

Wood handbook: wood as an engineered material. Madison, WI, USA: Forest Products Society; 1999.

Wu, Y., S. Wang, D. Zhou, C. Xing, Y. Zhang, G. M. Pharr. 2008. Use of nanoindentation and SilviScan to determine the mechanical properties of ten hardwood species. Wood and Fiber Science (Under review).

Xing, C., S. Wang, G. M. Pharr, L. S. Groom. 2007. Effect of thermo-mechanical refining pressure on the properties of wood fibers as measured by nanoindentation and atomic force microscopy. Holzforschung 62: 230-236.

Xing, C., S. Wang, G. M. Pharr. 2008. Comparison of the effects of the thermomechanical refining pressure on the properties of refined fibers of juvenile and mature wood. Wood Science and Technology (in print).

Yoshihara, H., and D. Yamamoto, 2004. Examination of compression testing methods for wood in the parallel to the grain direction. Forest Products Journal 54:56-60.

Yoshihara, H., and M. Ohta. 1997. Stress-strain relationship of wood in the plastic region III. Determination of the yield stress by formulating the stress-plastic strain relationship. Mokuzai Gakkaishi 43: 464-469.

Yoshihara, H., and S. Tsunematsu. 2007. Bending and shear properties of compressed Sitka spruce. Wood Science Technology 41: 117-131.

Yoshihara, H. and Y. Kubojima. 1998. Measurement of the shear modulus of wood by static bending tests. Journal of Wood Science 44: 15-20.

Zhang, H., B. E. Schuster, Q. Wei, K. T. Ramesh. 2006. The design of accurate micro-compression experiments. Scripta Materialia 54:181-186.

Zickler, G. A., T. Schoberl, O. Paris. 2006. Mechanical properties of pyrolysed wood: a nanoindentation study. Philosophical Magazine 86: 1373-1386.

VITA

Xinan Zhang was born in Changzhou, Jiangsu Province, China on October 6, 1980. He attended elemental and high school in Changzhou. He became a student at Nanjing Forestry University in 1999 and graduated with a Bachelor of Engineering degree in Wood Science and Technology in 2003. After that, he continued to study wood composites at Nanjing Forestry University and received his Master of Engineering degree in 2006. He came to study at University of Tennessee, Knoxville and received Master of Science degree in Forestry in August 2008.